運輸省港湾技術研究所 (25th Anniversary Issue)

港湾技術研究所報告

REPORT OF THE PORT AND HARBOUR RESEARCH INSTITUTE

MINISTRY OF TRANSPORT

VOL. 26 NO. 5 DEC. 1987

NAGASE, YOKOSUKA, JAPAN

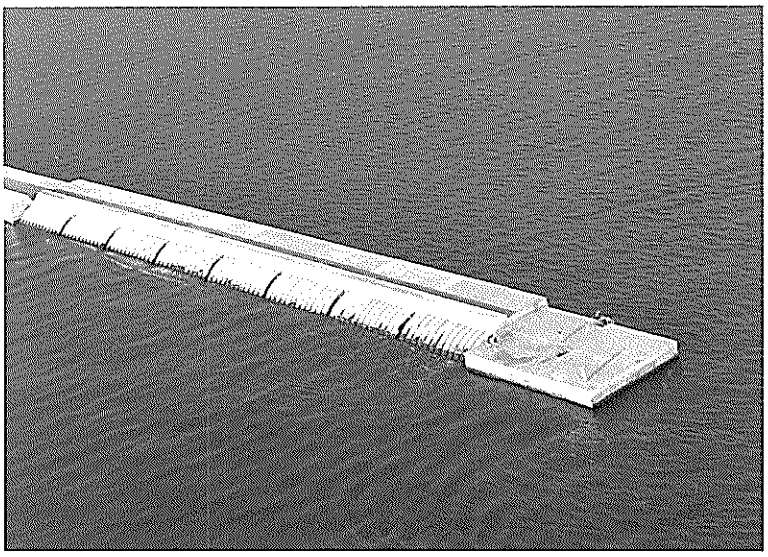

Curved Slit Caisson Breakwater

View of curved slit caisson breakwater completed in the construction at the port of Funakawa. (Courtesy of Akita Port Construction Office, the First District Port Construction Bureau, Ministry of Transport)

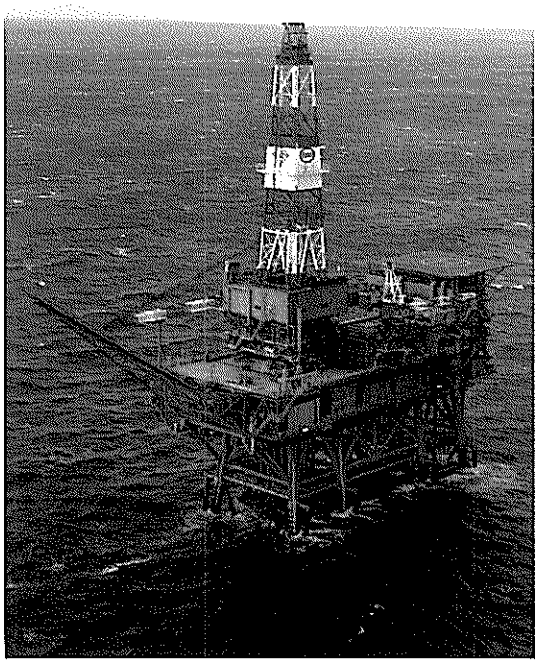

Facilities for Ocean Directional Wave Measurement

Four step type wave gauges and a two-axis directional current meter with a pressure sensor are installed on the legs of an offshore oil rig. They are operated simultaneously for detailed directional wave analysis.

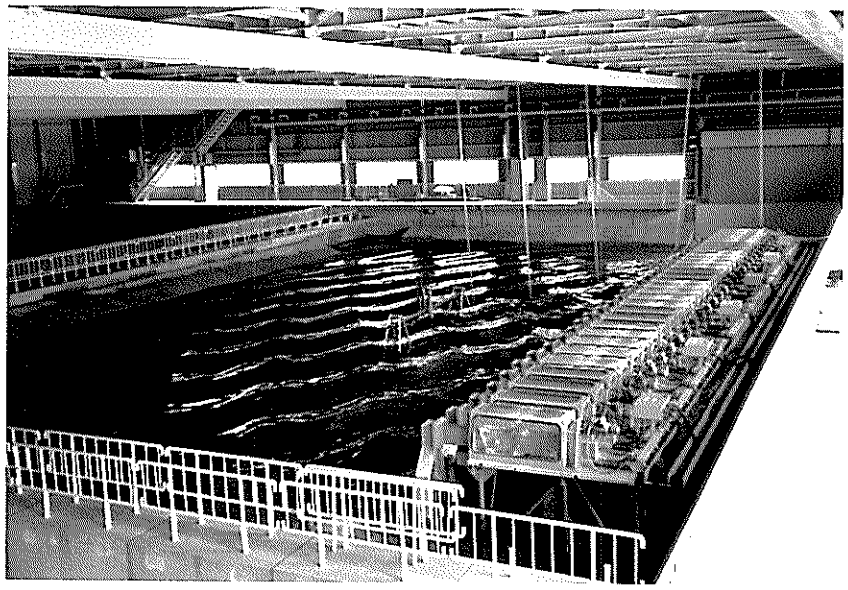

Serpent-type Wave Generator

The photograph shows the serpent-type wave generator in the short-crested wave basin and the superimposition state of two different oblique waves generated by the generator.

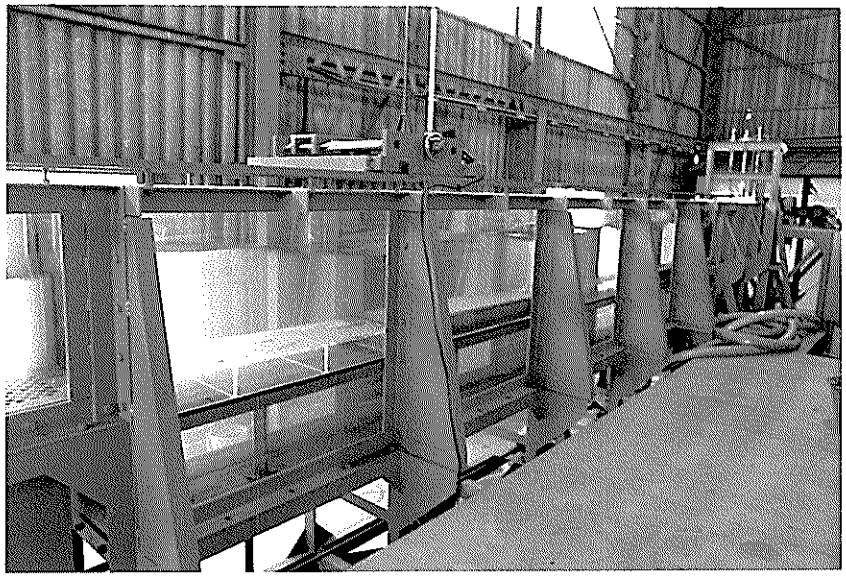

Wave-soil Tank

The experiments concerning the wave-soil interactions are conducted in this tank. The soil tank and the test section are located at the center of the tank. A movable floor is provided at the bottom of the test section and the level of the interface of mud layer and water can easily be adjusted to the level of the flume bottom.

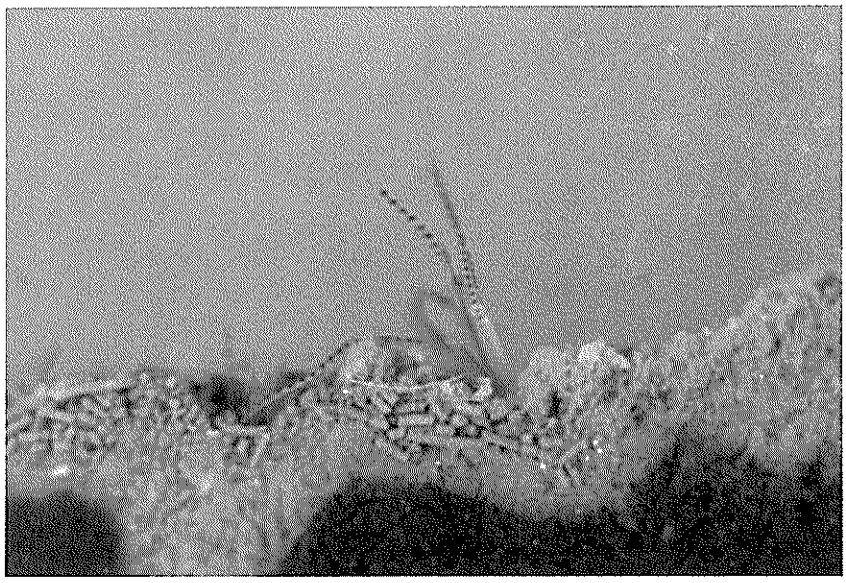

Pararionospio Pinnata

The biomass of benthos is one of the most sensitive indices to know the effect of sea-bed sediment treatments on the marine environmental improvement. The picure shows a kind of benthos, *pararionospio pinnata,* which preferentially exists in the polluted sea-bed.

Breakwater Damaged by Storm

This photograph shows a breakwater damage by a storm.
The breakwater is of the composite type with concrete caisson on a rubble mound. Two caissons were severly damaged due to the instability of a rubble mound.

Nondestructive Evaluation of Pavement

Nondestructive methods for evaluating the load carrying capacity of airport concrete pavements have been developed by using Falling Weight Deflectometer(FWD).

Seismic Damage to Gravity Quaywall

The 1983 Nipponkai-Chubu earthquake(Magnitude : 7.7)caused serious damage to port facilities in northern part of Japan. This photo shows the damage to gravity quaywall. The concrete cellular block walls were collapsed and completely submerged.

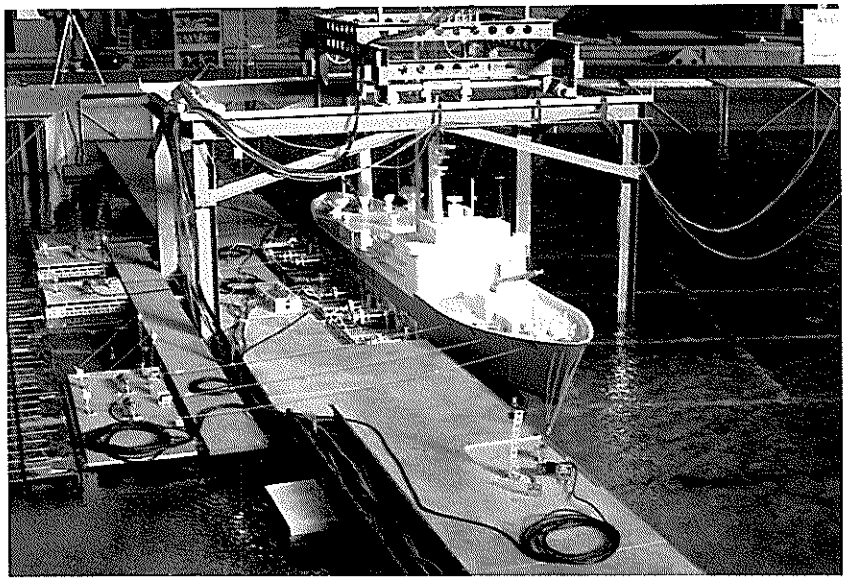

Model Experiment of Mooring Ship

Model ship is moored at a quay wall with fenders and mooring ropes subjected to gusty wind and/or irregular waves.

Vessel Congestion in Japan

As Japan is surrounded by the sea, there are many crowded water areas with various sizes and types of vessels. Arround there, many construction works were planned such as ports and harbours, off-shore airports, huge bridges and so on, so that many marine traffic observations and marine traffic simulations have been carried out.

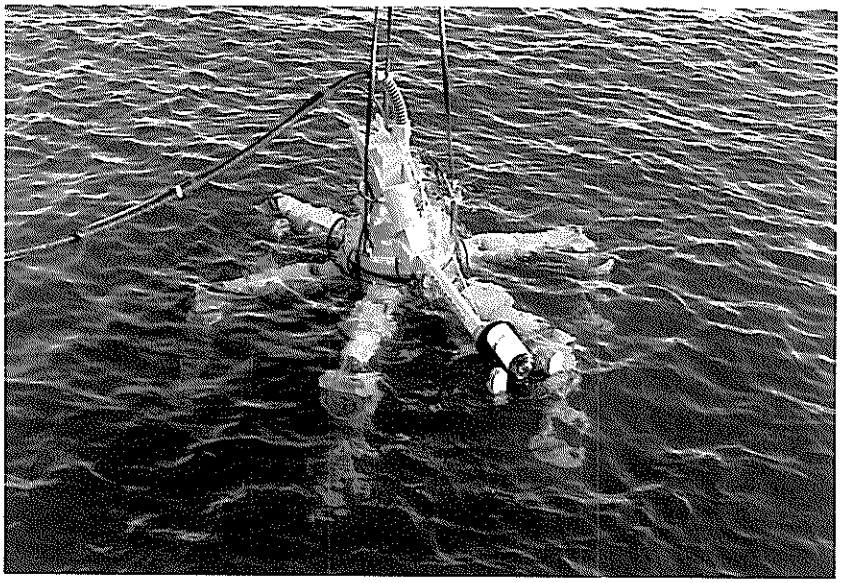

Underwater Inspection Robot

This is the six-legged articulated underwater inspection robot named "AQUAROBOT". The robot controlled by a computer can walk on uneven sea bed without making water muddy.

Foreword

The Port and Harbour Research Institute is a national laboratory under the Ministry of Transport, Japan. It is responsible for solving various engineering problems related to port and harbour projects so that governmental agencies in charge of port development can execute the projects smoothly and rationally. Its research activities also cover the studies on civil engineering facilities of air ports.

Last April we have celebrated the 25th anniversary of our institute because the present organization was established in 1962, though systematic research works on ports and harbours under the Ministry of Transport began in 1946. As an event for the celebration, we decided to publish a special edition of the Report of the Port and Harbour Research Institute, which contains full English papers only. These papers are so selected to introduce the versatility of our activities and engineering practices in Japan to overseas engineers and scientists. It is also intended to remedy to a certain extent the information gap between overseas colleagues and us.

The reader will find that our research fields cover physical oceanography, coastal and ocean engineering, geotechnical engineering, earthquake engineering, materials engineering, dredging technology and mechanical engineering, planning and systems analysis, and structural analysis. Such an expansion of the scope of research fields has been inevitable, because we are trying to cover every aspect of technical problems of ports and harbours as an integrated body.

The present volume contains eleven papers representing six research divisions of the institute. The materials introduced in these papers are not necessarily original in strict sense, as some parts have been published in Japanese in the Reports or the Technical Notes of the Port and Harbour Research Institute. Nevertheless they are all original papers in English and are given the full format accordingly. We expect that they will be referred to as usual where they deserve so.

It is my sincere wish that this special edition of the Report of the Port and Harbour Research Institute will bring overseas engineers and scientists more acquainted with our research activities and enhance the mutual cooperation for technology development related to ports and harbours.

December 1987
Yoshimi Goda
Director General

港湾技術研究所報告 (REPORT OF P. H. R. I.)
第26巻 第5号 (Vol. 26, No. 5) 1987年12月 (Dce. 1987)

目　　次 (CONTENTS)

REPORT OF THE PORT AND
HARBOUR RESEARCH INSTITUTE
Vol. 26, No. 5 (Dec. 1987)

6. Bearing Capacity of a Rubble Mound Supporting a Gravity Structure

Masaki KOBAYASHI*
Masaaki TERASHI**
Kunio TAKAHASHI***

Synopsis

In Japan, there are a large number of gravity structures rested on rubble mounds. The Japanese technical standards for designing port and harbour facilities have employed combinations of several formulae to analyse the stability of gravity structures on rubble mounds. This is due to the fact that there is no established formula for calculating the bearing capacity of rubble mounds including sub-soil under eccentric and inclined loads. Furthermore, the mechanical properties of rubble have not been well understood because of the difficulties encountered in laboratory shear tests.

Extensive research was carried out to clarify the bearing capacity of rubble mounds. This consisted of shear tests for rubbles by large triaxial apparatus, laboratory bearing capacity experiments by both a large scale model test and a centrifuge model test, field bearing capacity tests and investigation of the behaviour of actual gravity structures. The main conclusions can be summarized as follows:

(1) The shear strength of rubble is largely dependent on the confining pressure. This can be approximately simulated by introducing apparent cohesion.

(2) The ultimate bearing capacity by the simplified Bishop method agrees favourably with the results of both laboratory tests and field tests.

(3) Damaged and undamaged structures for composite breakwaters and gravity type wharves were examined. The simplified Bishop method gave reasonable results.

(4) The simplified Bishop method can be used for the unified formula for calculating the bearing capacity of a rubble mound including sub-soil under eccentric and inclined loads. In this case, it is recommended to introduce the apparent cohesion for rubble.

* Chief of Soil Mechanics Laboratory, Soils Division
** Chief of Soil Stabilization Laboratory, Soils Division
*** Chief of Foundations Laboratory, Soils Division.

港湾技術研究所報告
第26巻 第5号 (1987.12)

6. 重力式構造物の捨石マウンドの支持力

小林正樹*・寺師昌明**・高橋邦夫***

要　旨

本報告は捨石マウンド上の重力式構造物の支持力の検討を行うために，捨石の大型三軸試験，模型実験（大型模型実験および遠心載荷実験），現地実験および現地例の解析の結果を総合的に解析して新しい計算法の提案を行ったものである。それぞれの実験・調査からは下記のような結論が得られた。

(1) 砕石の三軸試験結果によると，石の強度は拘束圧によって大きく変化し，拘束圧が大きくなると強度が急激に減少する傾向が見られた。この傾向は見掛けの粘着力を導入することで近似できる。

(2) 大型模型実験によると，現行の設計法で規定されているような許容端し圧という固有な値は見られず，端し圧の値は荷重条件によって変化することが確かめられた。

(3) 各種の模型実験，現地実験および現地例の解析の結果によると，三軸試験の結果を用いて，ビショップ法による円形すべり計算を行えば現象を再現できることが明らかにされた。

本報告では，以上のような結論を基にして，捨石マウンド上の基礎の支持力の解析においてビショップ法を用いることを提案した。なお，石の強度としては，拘束圧依存性が大きいために，見掛けの粘着力を考慮し，$c=2$ tf/m², $\phi=35°$ を標準の値としている。さらに基礎地盤が砂の場合にも三軸圧縮試験を行うことを薦めているが，N値から ϕ を求める場合には，N値10以下で $\phi=40°$，N値10以上で $\phi=45°$ としている。

* 土質部　土性研究室長
** 土質部　地盤改良研究室長
*** 土質部　基礎工研究室長

Contents

1. Introduction

The total lengths of breakwaters and wharves in Japan currently amount to about 800 km and 1500 km, respectively. Most of the Japanese breakwaters are of the composite type with heavy concrete caissons resting on rubble mounds. About one third of the Japanese wharves are also the gravity structures resting on rubble mounds.

In designing a gravity structure it is necessary to predict the bearing capacity of the rubble mound and the sub-soil under inclined and eccentric loads due to the weight of a superstructure and the external forces of waves or earthquakes. Many general bearing capacity equations are available for the case of uniform stratum. However, they cannot be applied to predict the overall stability of a gravity structure resting on a rubble mound because the mound protrudes above the foundation and its geotechnical properties are different from those of the foundation. Furthermore the mechanical properties of rubbles have not been well understood because of the difficulties encountered in laboratory shear tests. In order to avoid these uncertainties the Japanese technical standards[1] for designing port and harbour facilities have employed the following complex procedures to predict the stability of gravity structures on rubble mounds:

1. The contact pressures of a caisson with the surface of rubble mound are calculated by assuming a linear stress distribution. The maximum contact pressure called the toe pressure must not exceed the allowable toe pressure, which has usually been taken at 40 tf/m^2 to 50 tf/m^2 based on past experience.
2. The pressure exerted by the superstructure and the rubble mound to the sub-soil is calculated by assuming that the distribution angle is 30°. Conventional bearing capacity equations for vertical loads are applied to predict the bearing capacity of the foundation at the bottom of the rubble mound.
3. Circular arc analysis is used to predict the bearing capacity of the foundation as a two-layer stratum (mound and subsoil). In this procedure, the shear strength parameters have been determined on the basis of case histories of damaged breakwaters and wharves.[2]

These procedures are highly empirical because the allowable toe pressure is not derived from bearing capacity theory and because the shear strength parameters are not accurately estimated. Consequently their application has been limited to structures for which we have much experience of stability analysis. Recently there are several large projects which call for the construction of large gravity structures at great water depths. For example, in order to protect the coast line of northern Japan against earthquake-originated Tsunamis, a huge breakwater with a 35 m high rubble mound is now being constructed at the water depth 60 m.[3] In these cases empirical stability analysis based on the allowable toe pressure tends to dictate an excessively safe design and leads to the unnecessary rise of the construction cost.

In order to clarify the stability of gravity structures on rubble mounds, we have carried out extensive investigations. The first important point is to understand the mechanical properties of rubble. Thus, large triaxial tests of various rubble were carried out. Subsequently, in order to clarify the bearing capacity of rubble mounds, two types of laboratory model tests were performed; a large scale model test where actual rubbles were used and a centrifuge model test which

satisfies the similarity. Furthermore, field loading tests were carried out at two locations.

In this paper the results of each investigation are described, and through verification with prototype data, we propose a new method for predicting the bearing capacity of a rubble mound supporting a gravity structure.

2. Mechanical Properties of Rubble

2.1 Rubble in Actual Use[4]

In order to study the mechanical properties of rubble for the port construction work in Japan, rubble in actual use is investigated first. Rubbles chosen for the investigation are so-called foundation rubble that form a base sustaining the heavy weight of breakwater. Each port construction bureau has its own specifications for rubble used in port construction works. These specifications have been empirically made in consideration of each regions' conditions such as the demand for rubble in a region and the conditions of the rubble production sites, and the construction works.

Four representative rubble production sites were selected, one for each construction bureau, and the rubble from each of the four sites was examined for its mechanical properties, weight distribution, and shape of the individual grains. The weight distributions are shown in Fig. 1 as four curves with the names of their production sites. In order to obtain the grain size distributions, the correlation between the weight and the intermediate size of single grains is examined. Figure 2 shows the correlation representing the case for Iwaki; the other three cases also have close relations. Figure 3 shows the grain size distributions which are obtained from each weight distributions through the respective correlations. The values of the uniformity coefficients U_c for the four kinds of rubbles are 1.3–2.5, which are

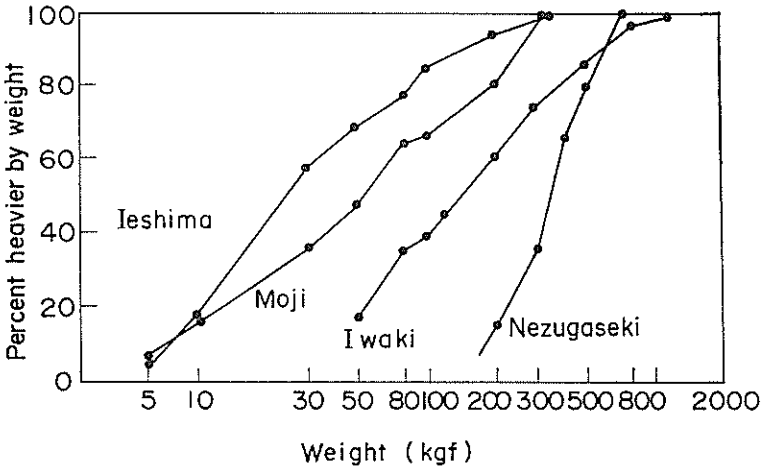

Fig. 1 Grain Weight distribution curves of four kinds of actual rubbles

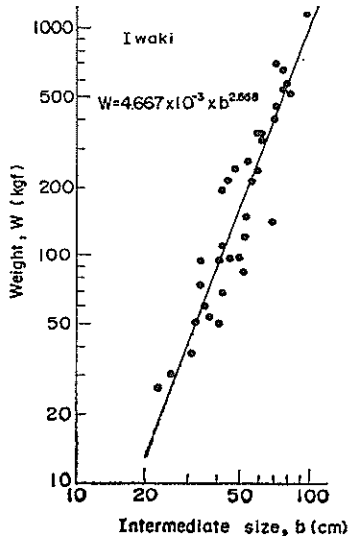

Fig. 2 Relationships between weight and intermediate size of single grains

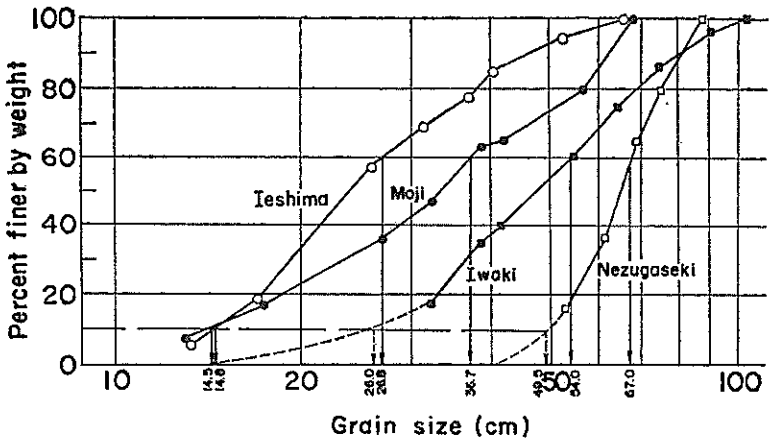

Fig. 3 Grain size distribution curves

smaller than those of rocks used for fill-type dams.[5]

2.2 Mechanical Properties of Rubble

In order to study the mechanical properties of rubble, two kinds of triaxial compression tests are carried out, i.e., one with middle size specimens 30 cm in diameter by 60 cm in height, and the other with large size specimens 1.2 m in diameter by 2.4 m in height. The source rocks for the two kinds of rubbles tested are granite and hard sandstone; their specific gravity is more than 2.6 and their

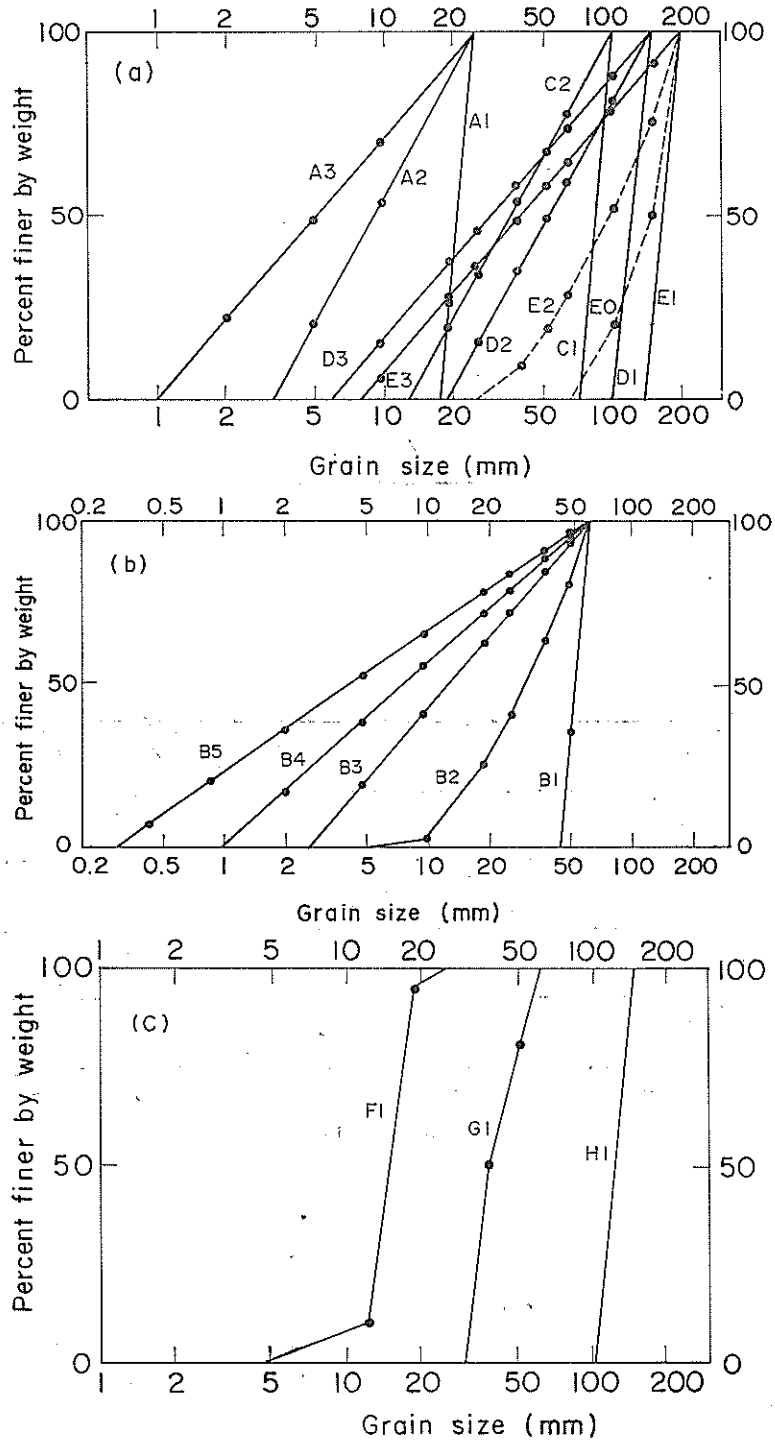

Fig. 4 Grain size distribution curves of rubbles tested

Table 1 Triaxial compression test program

Source Rocks	Specimens	D_{max}	Case	U_c	Confining Pressure σ_3 (kgf/cm²)		
					Loose	Medium	Dense
Granite	Middle Size (d=30 cm, h=60 cm)	25.4	A 1	1.2	2, 4		
			A 2	2.8	2, 4		
			A 3	5.0	2, 4		
		63.5	B 1	1.2	2, 4	1	1, 2, 4
			B 2	2.8		1, 2, 4	1, 2, 4
			B 3	5.0	1, 2, 4		1, 2, 4
			B 4	8.0	1, 2, 4	1, 2, 4	1, 2, 4
			B 5	15.0		1, 2, 4	1, 2, 4
	Large Size (d=1.2 m, h=2.4 m)	100	C 1	1.2	2		
			C 2	2.8	2		
		150	D 1	1.2	2, 4, 8	1, 2, 4, 8	
			D 2	2.8	2		
			D 3	5.0	2		
		200	E 1	1.2	2		
			E 0	2.0			4
			E 2	2.8		4	1, 2, 4
			E 3	5.0	2		
Hard Sandstone	Middle Size	25.4	F 1	1.3	2, 4, 8	0.5, 1, 2, 4, 8, 14	2, 4, 8
		63.5	G 1	1.3		2, 4, 8	
	Large Size	150	H 1	1.2		2, 4, 8	

unconfined compressive strength is 1400–1700 kgf/cm². The conditions varied in the test are maximum grain size and grain size distribution, as shown in Fig. 4; the grain size distributions are similar to those of the actual rubbles shown in Fig. 3. The density of rubble and the confining pressure were also varied in the series of tests, as shown in Table 1.

(1) Influence of Confining Pressure[4]

Figure 5 shows influence of effective confining pressure σ_3 on the shear strength ϕ_0. The shear strength ϕ_0 is defined as $\sin\phi_0=\{(\sigma_1-\sigma_3)/(\sigma_1+\sigma_3)\}_f$, where σ_1 and σ_3 at failure are defined as those values at axial strain of 15% if the axial stress shows no peak values. The characteristic of the shear strength decreasing with increasing confining pressure is closely related to grain breakage and the dilatancy characteristics.[6]

Figure 6 shows the same influence of the standard sand (Toyoura sand)[7]. While the same tendency can be seen for the sand also, comparison of Figs. 5 and 6 indicates a marked decrease in the shear strength of rubble at a low confining pressure.

(2) Influence of Grain Breakage[4]

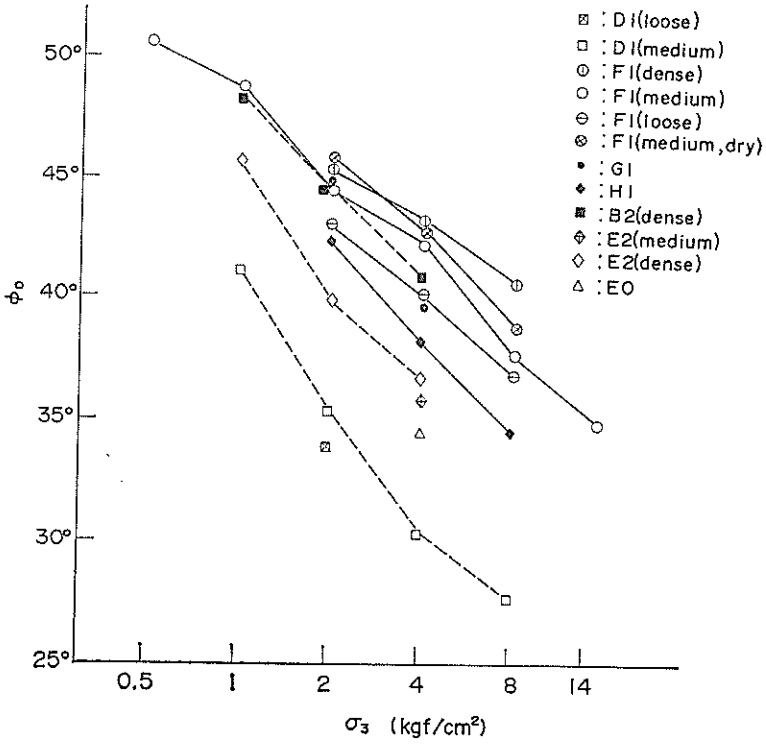

Fig. 5 Relationships between shear strength and confining pressure (rubble)

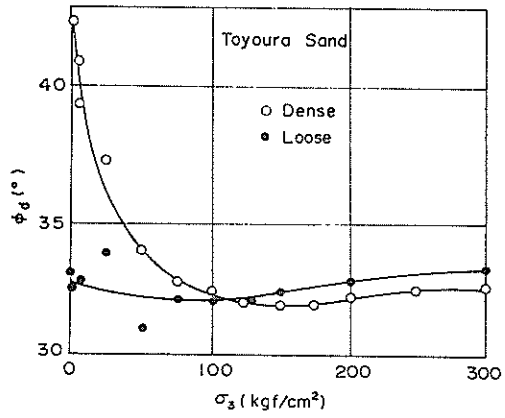

Fig. 6 Relationships between shear strength and confining pressure (sand)

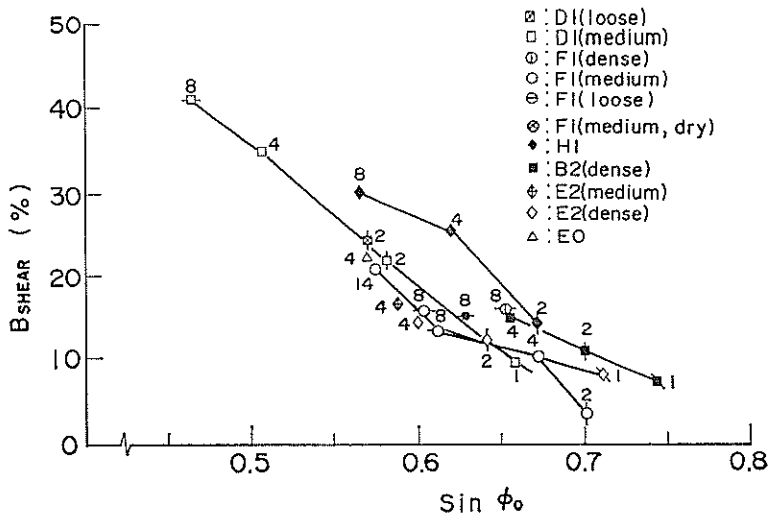

Fig. 7 Relationships between grain breakage and shear strength (values besides the points means σ_3)

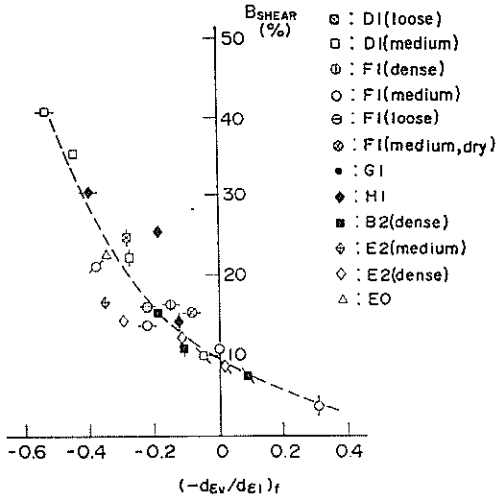

Fig. 8 Relationships between grain breakage and dilatancy ratio

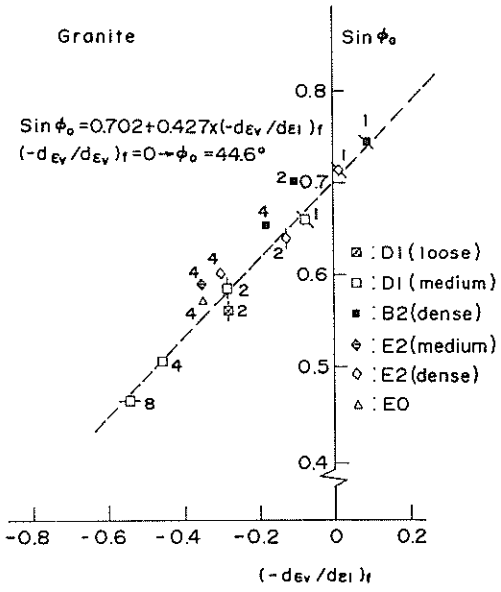

Fig. 9 Relationships between shear strength and dilatancy ratio (values besides the points means σ_3)

Figure 7 shows the correlation between the shear strength $\sin\phi_0$ and grain breakage B_{shear}, where the grain breakage is expressed by the index after Marsal[8]. It reveals that the shear strength increases as the grain breakage lowers.

The dilatancy ratio at failure $(d\varepsilon_v/d\varepsilon_1)_f$ is plotted against the grain breakage in Fig. 8 and against $\sin\phi_0$ in Fig. 9. These Figures indicate that a high grain breakage keeps the dilatancy ratio negative and makes the shear strength low.

(3) Influence of Maximum Grain Size[9]

Relative density is a significant factor for the shear strength of granular materials such as rubble. In order to calculate the relative density, the maximum and minimum densities are necessary. The minimum density is, however, difficult to obtain because of easy breaking of the grains. In the present study we carried out compaction tests for rubble, and define the minimum void ratio as the void

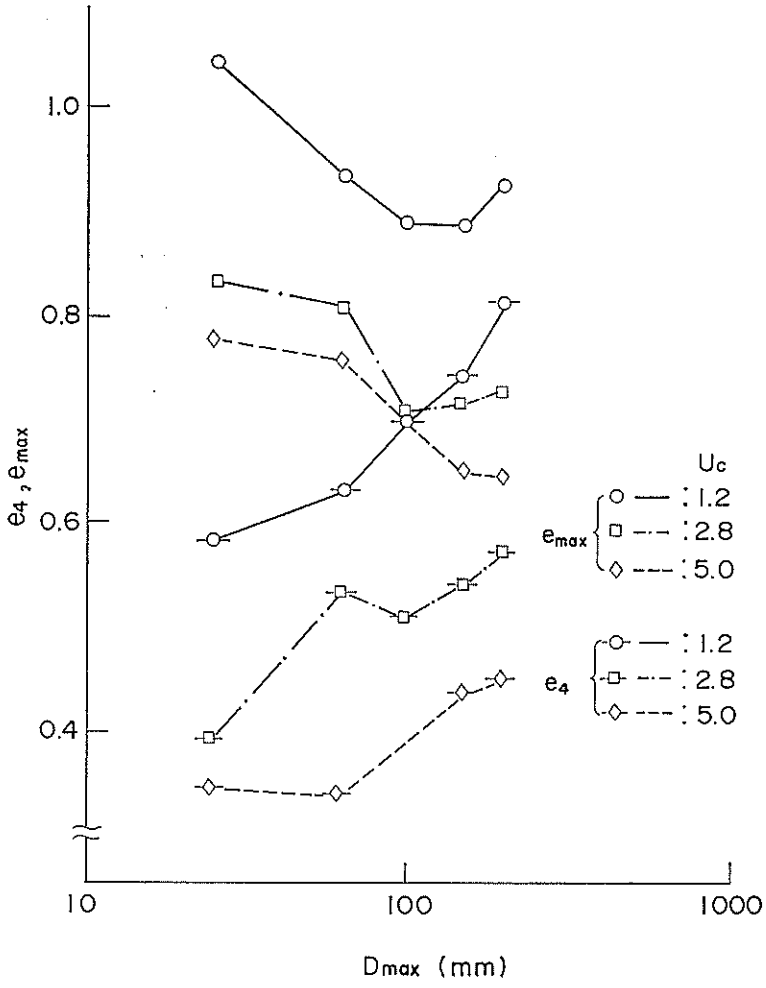

Fig. 10 Relationships between maximum and minimum void ratios and maximum grain size

ratio obtained after compaction for 4 minutes that is expressed by e_4, which includes negligible grain breakage and which seems to be as close as possible to the most dense condition. Relative densities D_r' calculated using e_{max} and e_4 as e_{min} are 45–55% for the loose condition, 60–80% for the medium condition, and 100–120% for the dense condition.

Figure 10 shows the variations of the maximum void ratio e_{max} and the minimum void ratio e_4 defined above with the maximum grain size D_{max}. It indicates that the range of possible void ratio becomes narrow with increasing D_{max}. Figure 11 shows the correlations between D_{max} and e_{50} (void ratio when relative density is 50% based on e_4). The variation of e_{50} is small.

Figure 12 shows the correlations between D_{max} and ϕ_0 under the condition of σ_3= 2 kgf/cm². Only a slight change in ϕ_0 is observed for each U_c. This fact is important because it indicates that ϕ_0 of actual rubbles with sizes too large to test, is the same as ϕ_0 from the tests of small grain sizes of the same U_c as the actual rubbles.

(4) Influence of Uniformity[9]

Figure 13 shows the variations of the maximum void ratio and minimum void ratio with U_c; the influence of U_c on the maximum and minimum void ratios is revealed to be significant.

Figure 14 shows the correlations between U_c and the grain breakage index after Marsal during the process of consolidation and test at σ_3=4 kgf/cm². Significant grain breakage appears with the decrease of U_c.

Figure 15 shows the correlations between U_c and ϕ_d which is determined from the test results for the three confining pressures: 1, 2, 4 kgf/cm². It is indicated that ϕ_d increases with increasing U_c. The values written beside the points in Fig. 15 are the sum of the grain breakage during the process of consolidation and testing at the three confining pressures. These values indicates the same facts seen in

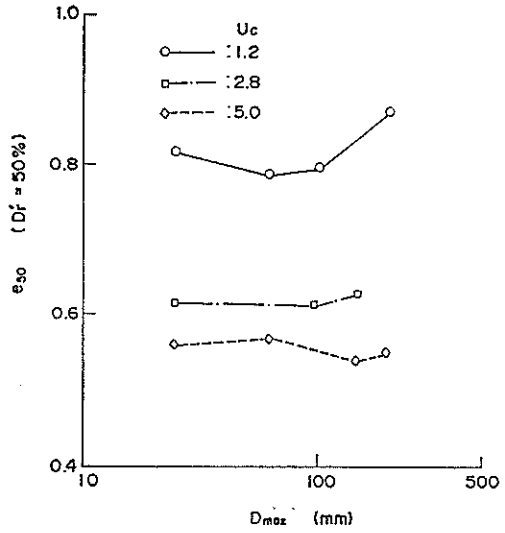

Fig. 11 Relationships between D_{max} (maximum grain size) and e_{50} (void ratio when D_r'=50%)

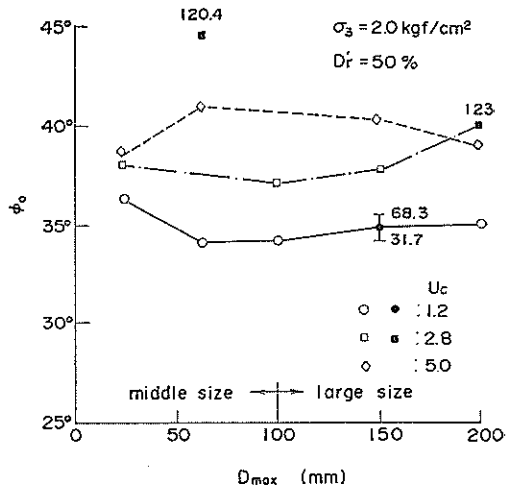

Fig. 12 Relationships between D_{max} (maximum grain size) and ϕ_0 (values besides the points means D_r', for the points without values D_r'=50%)

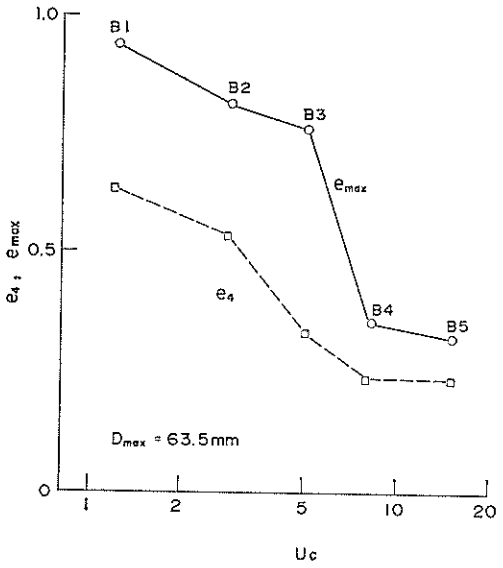

Fig. 13 Variations of maximum (e_{max}) and minimum (e_4) void ratios with uniformity coefficients (U_c)

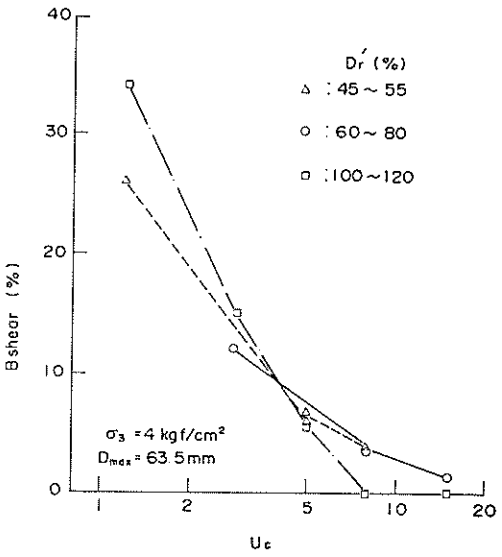

Fig. 14 Relationships between U_c and grain breakage during the process of consolidation and test

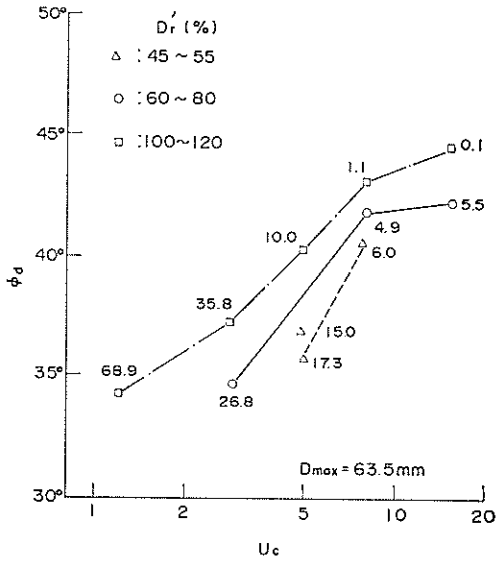

Fig. 15 Relationships between U_c and ϕ_d determined from test results of three confining pressures 1, 2, 4kgf/cm²

Fig. 14.

3. Large Scale Model Test

3.1 Contents of Model Test[10]

(1) Apparatus of Model Test

The large scale model test is schematically shown in Figs. 16 and 17. The test is carried out in a rigid steel tank having the dimensions shown in Fig. 16. Only the base plane of the breakwater caissons is represented by a thick steel plate having dimensions of 1.9 m×1 m×20 cm. The two kinds of plate used have base surface of different roughness, with the coefficients of friction 0.4 and 0.6. The plate is loaded vertically and horizontally in various combinations. For vertical loading one

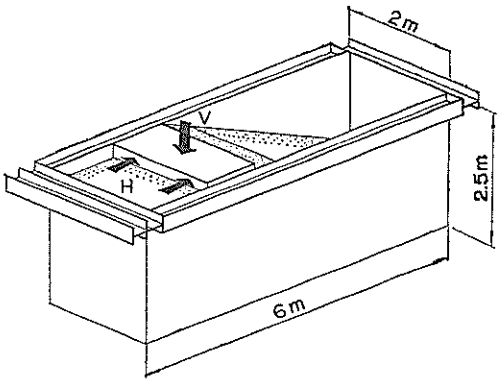

Fig. 16 Large scale model test (cases for slope mound)

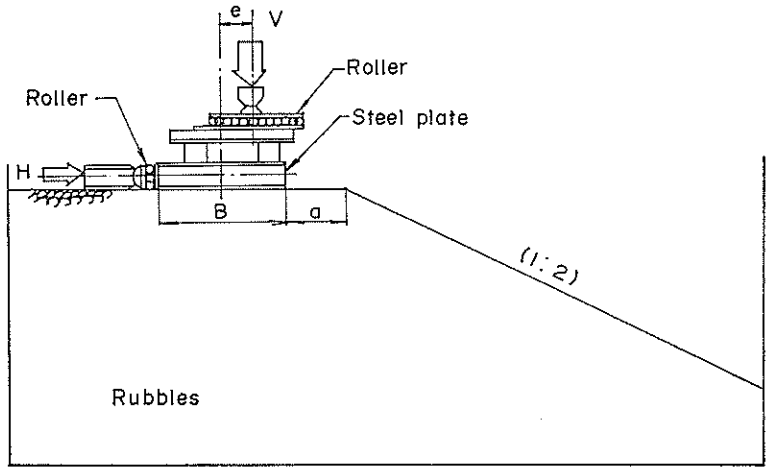

Fig. 17 Large scale model test (cases for slope mound)

Table 2 Large scale model test program

Case	Eccentricity (ε_t)	Inclination ($\tan \alpha_i$)	Mound Shape	Friction Coefficient	Symbols
A—1	0	0	Horizontal	0.4	○
2	0	0	〃	〃	○
B—1	0.33	0	〃	0.4	◎
C—1	0.48	0.33	〃	0.4	△
2	〃	〃	〃	〃	△
3	〃	〃	〃	0.6	△
4	〃	〃	〃	〃	△
5	〃	〃	〃	〃	△
6	〃	〃	〃	〃	△
I—1	0.48	0.45	〃	0.6	⊡
D—1	0.33	Increase (V=100 tf)	〃	0.4	☆
2	〃	Increase (V=150 tf)	〃	〃	☆
3	〃	Increase (V=200 tf)	〃	〃	☆
E—1	0.48	0	Slope(a=50 cm)	0.6	●
F—1	0.48	0.33	〃	0.4	▲
2	〃	〃	〃	0.6	▲
3	〃	〃	〃	〃	▲
G—1	0.48	0.20	〃	0.6	■
2	〃	〃	〃	〃	■
H—1	0.48	0.33	Slope (a=100 cm)	0.4	▲
2	〃	〃	〃	0.6	▲

big hydraulic jack is used, and two hydraulic jacks are used for horizontal loading. The loads are made truly vertical or horizontal with use of the devices illustrated in Fig. 17.

(2) Series of Model Test

As listed up in Table 2, the conditions varied in the test are the eccentricity and the inclination of the total loads and the breadth of slope top a shown in Fig. 17.

The eccentricity ε and the inclination $\tan\alpha$ of the total loads are expressed in dimensionless forms: $\varepsilon=2e/B$, $\tan\alpha=V/H$ (e, B, V, and H are illustrated in Fig. 17). As the steel plate moves by the loads, ε changes in the process of the test. The values listed up in Table 2 are the initial ones, and have the subscript i. The meaning is the same with $\tan\alpha_i$.

(3) Process of Model Test

The vertical load and the horizontal load are increased simultaneously in the way that $\tan\alpha$ is the same as $\tan\alpha_i$ in Table 2. Only in case D, the vertical load is kept at the prescribed magnitude and the horizontal load is increased. Consequently, the inclination of the total load increases.

(4) Rubble Mound in Model Test

As the rubble mounds in the model test are made by compacting in the prescribed way, the unit weights of them are almost the same value i.e. 1.55 tf/m^3. After the tests, larger values of 1.6–1.8 tf/m^3 are measured under the steel plate. It is caused by compaction with crushing of rubble during the test.

3.2 Results of Model Test

(1) Displacement of the Steel Plate[10]

For discussing the displacement of the steel plate, it is convenient to use the composite displacement of the vertical and horizontal displacements. The composite displacement δ means that of the edge at forward and base surfaces. In the same

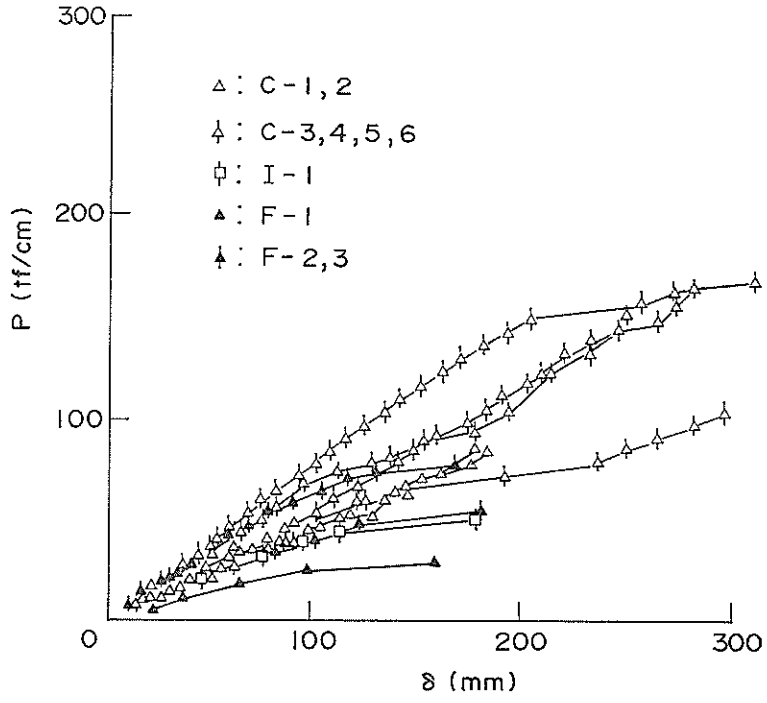

Fig. 18 Relationships between composite load P and composite displacement δ

meaning, the vertical and the horizontal loads are composed into the total load P. A few examples of the relation between the composite displacement and the composite load are illustrated in Fig. 18. These curves indicate the differences resulting from the eccentricity of the load and from the shape of the rubble mound.

(2) Examination through Toe Pressure[10]

The eccentricity changes significantly in the process of the test and consequently the distribution of the reaction forces of the rubble mound also changes. The calculated toe pressure p_1 is illustrated in Fig. 19 in order to examine this change of reaction force distribution. These curves for the initial eccentricity of 0.48 show maximums between the first increases and following decreases on the abscissa of the composite displacement. These phenomena are observed in the curves for all the other conditions.

Figure 20 shows the relationships between p_1 and eccentricities ε_{cr} at the maximum points in Fig. 19. Figure 21 shows the relationships between p_1 and inclinations $\tan \alpha_f$ at the last points of the tests. These figures indicate that toe pressure decreases with the increase of either the eccentricity or the inclination. Furthermore, the clear difference between the open marks for the horizontal grounds and the solid marks for the sloping grounds in Fig. 21 reveals that the sloping grounds have a smaller maximum toe pressures and consequently smaller bearing capacities than the horizontal grounds. The influences of the eccentricity and the inclination of the total load and the shape of the rubble mound are clarified in these figures.

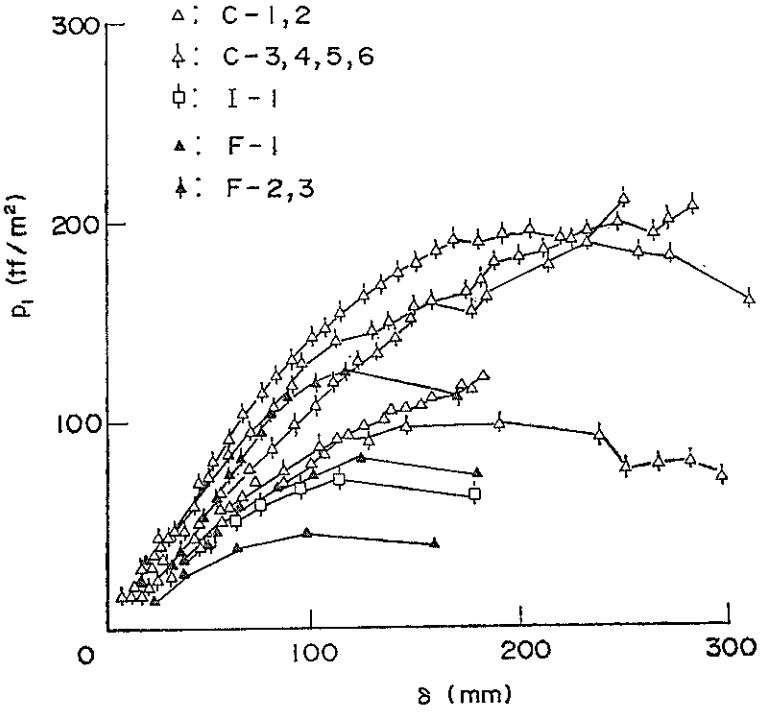

Fig. 19 Relationships between calculated toe pressure p_1 and composite displacement δ

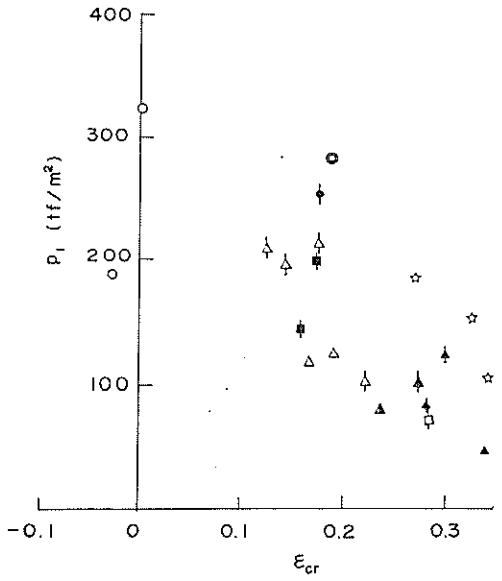

Fig. 20 Relationships between calculated toe pressure p_1 and eccentricity ε_{cr} at the maximum points in Fig. 19

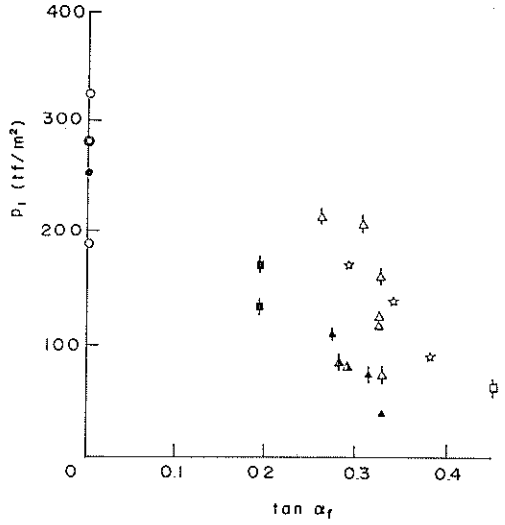

Fig. 21 Relationships between calculated toe pressure p_1 and inclination $\tan\alpha_f$ at the last points of test

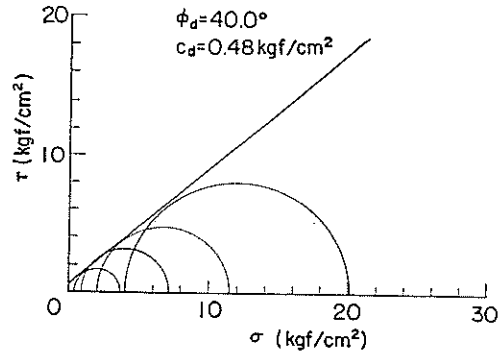

Fig. 22 Results of triaxial compression test

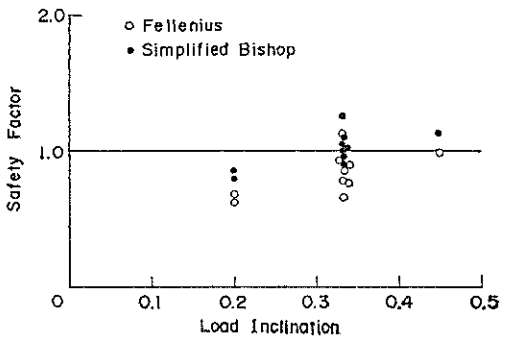

Fig. 23 Analysis by the simplified Bishop circular arc method

(3) Analysis by Circular Arc Method

In order to analyze the test results precisely, it is necessary to consider the shear strength ϕ to be the function of the confining pressure, because ϕ of the rubble of the test mound changes widely according to the confining pressure. However, this consideration is too complicated for actual use. Therefore, we used the shear strengths c=0.48 kgf/cm² and ϕ=40° which were obtained from the triaxial compression tests; confer Fig. 22. The use of the apparent cohesion c can express the influence of confining pressure on ϕ to some extent.

Figure 23 shows the safety factors from the circular arc method by Fellenius and

from the simplified circular arc method by Bishop using the above shear strengths for the limited data that have peak values. While the safety factors by Fellenius method are too small, the safety factors by the simplified Bishop method are close to 1. Consequently, the test results are well explained by the simplified Bishop method.

4. Centrifuge Modeling of a High Sand Mound

The study described in the present section is of rather a fundamental nature which deals with the bearing capacity of shallow foundations on top of high sand mounds under eccentric and inclined loads. The term "high" is used because the major object of the study is limited to sufficiently high mounds where the failure load is not influenced by the condition of the soil under the mound. The final target of the study is to find out the most appropriate practical design technique which can reasonably explain the influence of the slopes on both sides of the mound, the load eccentricity, and the load inclination on the bearing capacity.

In such a study, it is necessary to carry out model tests which satisfactorily represent the prototype-scale behavior. All the model tests are carried out in the plane strain condition in the high acceleration field by means of a geotechnical centrifuge. As the details of the study have already been reported in the separate publication[11], only the major points are discussed here.

4.1 Test Conditions and Test Procedure

(1) The centrifuge and strong specimen box

The radius of the PHRI centrifuge is 3.8 m when measured to the surface of swing platform. The maximum payload is 2.7 tons and the maximum acceleration is 115 g. This, the maximum capacity of the machine is 300 g-tons. The details of the PHRI geotechnical centrifuge and ancillary equipment were reported in a separate publication[12].

The high sand mound is reduced in scale and prepared in a strong specimen box, which has inside dimensions 30 cm deep, 10 cm wide, and 100 cm long. One side of the strong box is made of glass to allow photographic measurement by a 70 mm data camera and real time observation by television.

(2) Model ground and model foundation

The material used for the mound is Toyoura sand which is a fine uniform sand having a uniformity coefficient U_c of 1.38 and an effective grain size D_{10} of 0.13 mm. The sand is used because of its well known characteristics and relative ease in preparing model mounds of desired density. The model ground of Toyoura Sand is prepared in the strong box on the laboratory floor by means of the multiple sieve method of sand raining. The relative density of the sand is controlled to within 94–100%. The corresponding ϕ value obtained by the conventional triaxial compression tests (ϕ_{tr}) is 40 to 46 degrees and the ϕ value in the plane strain condition (ϕ_{pl}) is 47.5 to 52 degrees[13]. The higher ϕ value corresponds to a low confining pressure and a lower ϕ value corresponds to a high confining pressure in each test condition. The slopes of the mounds are excavated by sucking sand particles by vacuum pump. The gradient of the slope is taken as one vertical to two horizontal.

The model foundation is made of aluminum with high rigidity. The base of

the foundation is glued with the same sand as that used for the model ground to represent the rough base condition.

(3) Size of model foundation and applied acceleration

The present model tests have no specific prototype. However, the model test conditions cannot be determined without an insight into the prototype conditions. If a small foundation is used to determine the bearing capacity of a sufficiently large foundation, the bearing capacity obtained by the model overestimates the actual bearing capacity. This is the well known scale effect for the bearing capacity problems. A series of concentric vertical loading tests on the flat ground of Toyoura Sand are performed to determine the size of a model foundation and the acceleration to be applied in the model test[14]. Generally, the length B in the model under $N\,g$ corresponds to the length B^*N in the prototype. Rough-base foundations with various breadths are loaded vertically in the various acceleration fields. A unique relationship between the bearing capacity factor N_γ and B^*N is obtained from the test results regardless of the actual model foundation width B when it exceeds 2 cm. Due to the scale effect, N_γ decreases with increasing B^*N, and becomes constant when B^*N exceeds 100 cm. Thus, the width of the model foundation and the acceleration is selected to be 4 cm and 60 g respectively throughout the model tests in order to enable the simulation of sufficiently large foundations such as upright sections of breakwaters.

(4) Mound height and location of foundation

As described earlier, the scope of the study in the present section is limited to the shallow failure which occurs in the high mound. It means that the mound is high enough to avoid the influence of sub-soil condition on the bearing capacity of the foundation. And also, the foundation must be close enough to the edge of the mound to enable the determination of the influence of the sloping sides of the mound on the bearing capacity.

To find out appropriate distance (W) of the foundation from the edge and the appropriate mound height (H), concentric V-load tests on the symmetric mounds are carried out changing W/B and H/B, in advance of the eccentric inclined loading tests. Based on the test results, W/B is determined to be 0.25 and 1, and H/B to be 3 for the main experiments under eccentric V-load and H-load.

(5) Loading condition and loading equipment

In order to model the upright section of the breakwater which has freedom to be displaced in any directions, the model foundation must also have the freedom to be displaced in any direction. Any loading condition at the base of the foundation can be converted to a combination of a vertical load component (V) with a certain eccentricity (e) and a horizontal load component (H). A new loading equipment is devised as shown in Fig. 24. By the new equipment, a vertical load component is given to the foundation via steel bearing and a horizontal load component is given by wire tension through hinges so as not to cause any restriction on the displacement and rotation of the foundation.

The test procedure using new equipment is as follows. The loading equipment including the model foundation is mounted on the strong box. The foundation is hung over the top surface of a mound approximately at the center line of the mound. The steel bearing is installed between the foundation and the load cell at the approximate position for the prescribed eccentricity. The strong box is mounted on the platform of centrifuge. Until the prescribed acceleration is reached, the

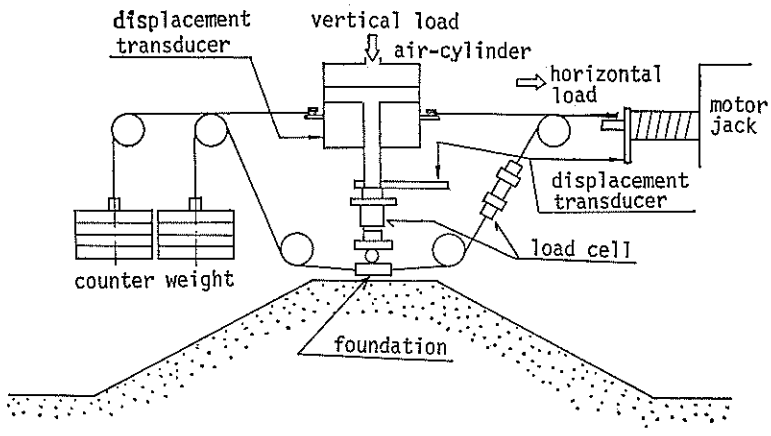

Fig. 24 Loading Equipment

foundation is kept hanging over the mound. At a constant acceleration, the position of the foundation is adjusted exactly to the center line of the mound. The V-load with a certain eccentricity is given by an air-cylinder and the foundation lands on the top surface of the mound. Then, finally, the H-load is applied to the foundation and is increased to failure of the mound at a constant displacement rate. To avoid the excessive change of eccentricity during the experiment, the air-cylinder is also pulled by the wire at the same horizontal displacement rate as that of the foundation. During the experiment, the vertical load at the loading point, the tension in the wire, the vertical displacement of loading point, and the horizontal displacement of the foundation are directly measured by transducers.

4.2 Centrifuge Test Results

(1) Failure envelope

23 model tests are carried out under the eccentric and inclined load. The loading condition at the base of the foundation is given in the model tests as a combination of the vertical load component V with a certain eccentricity e and the horizontal load component H. The same loading condition can be converted to a combination of the concentric vertical load component V and the horizontal load component H at the foundation base and the moment about a center of the foundation base. For convenience in discussions, a set of V, H and M is used in the following paragraphs. However the same symbols V and H will be used because the magnitudes of V and H do not change by this conversion. The moment M about the center of the foundation base is the product of V and e.

By the test results, a failure envelope may be constructed in the V–H–M space for a particular geometric condition. When the test data ($W/B=1$, $H/B=3$) with negligible eccentricity are projected into the $M=0$ plane and plotted by the solid circles, Fig. 25 is obtained. In the figure, two data obtained previously by the tests for a vertical concentric loading which correspond to $W/B=1$ and $H/B=3$ are also plotted on the V-load axis. The eccentricity of the each data point in the figure differs slightly but within the range of $-0.1<e/B<0.1$. For convenience, the data with positive e/B are plotted on the upper half and the data with negative e/B are

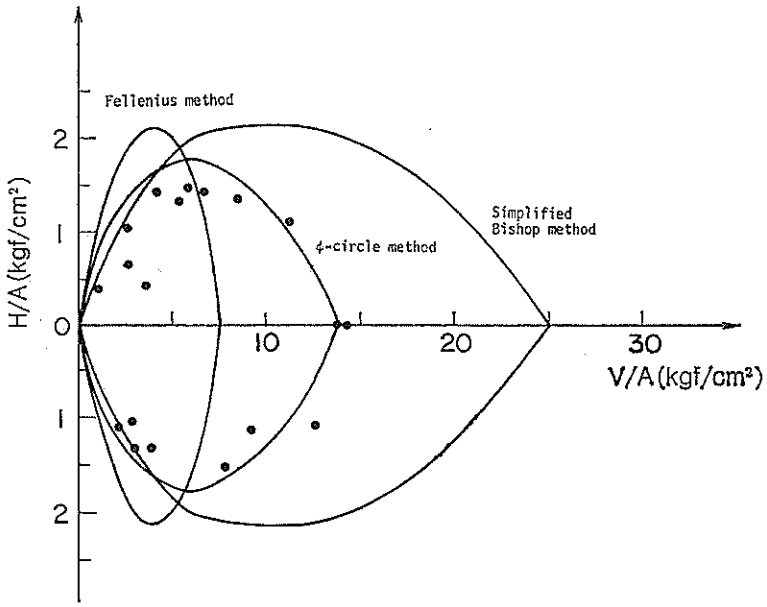

Fig. 25 Projected Data on M=0 Plane with Calculations ($\phi=45°$)

plotted in the lower half of the figure. The plotted data group on the plane has a shape of cross section of a spindle. The maximum horizontal load can be found at the vertical load level of approximately one half of the maximum vertical bearing capacity.

(2) Horizontal load intensity—displacement relation

Relationships between the horizontal load intensity and the horizontal displacement of the foundation are influenced by the applied vertical load level as shown in Fig. 26. The H-load intensity and H-displacement curve for a lower vertical load level, as shown by open circles, has no clear peak. However, the curve for a higher vertical load level, as shown by open triangles, has a sharp peak at small displacement and shows a sudden reduction of resistance. The vertical load level for the curve shown by solid circles is between those for the above two curves and corresponds to approximately one half of the maximum vertical load sustained by the present mound. In this case the highest horizontal resistance can be mobilized for this particular geometric condition of the mound.

(3) Displacement and Rotation of the Foundation

Displacements of the foundation in the vertical and horizontal directions are measured during model tests with a certain time interval. It is interesting to see the increment of displacement within a time interval starting from the instance of failure in order to understand the mode of failure. The displacement increment vectors at the failure loads are shown in Fig. 27 together with the failure loads again for the cases where e nearly equal to zero. In the figure, the ordinate shows the horizontal load intensity at failure, and the abscissa shows the vertical load intensity. Solid circles in the figure represent the failure loads. The origin of the displacement increment vector for a certain test condition is taken at the corresponding point of

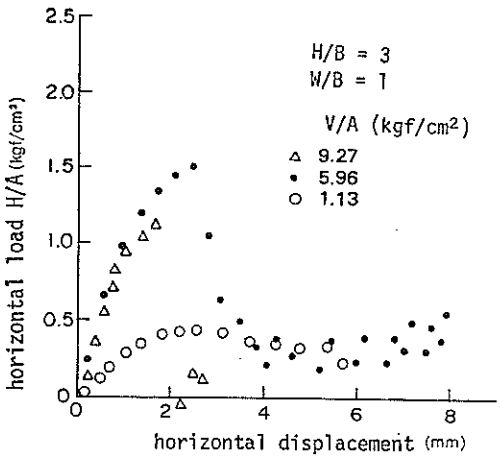

Fig. 26 Typical Examples of Load-Displacement Relationship for the Case with Negligible Eccentricity

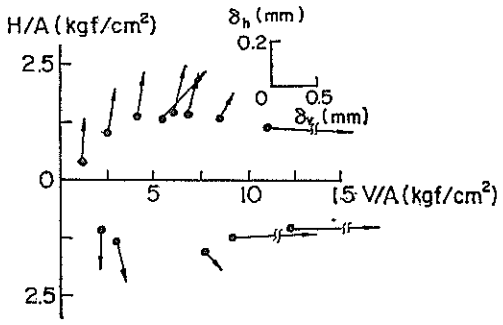

Fig. 27 Displacement Increment Vector at Failure

failure loads. The directions and magnitudes of the vertical displacement increment (δ_v) and horizontal displacement increment (δ_h) are shown in the figure. In the lower V-load level, the displacement increment vector is parallel to the δ_h axis, which means that the slip surface appears at shallow depth and the failure mechanism of the mound in this range is close to the sliding of the foundation. In the higher V-load level, the displacement increment vector is almost parallel to the δ_v axis, which suggests that the bearing capacity failure occurs although the horizontal load brings the foundation to failure.

Inclination of the foundation from horizontal plane at failure is measured from photographs for each test condition. The magnitude of the inclination is found to be roughly proportional to the magnitude of the moment component.

4.3 Discussions

(1) Comparison of the test results with calculation

In the present study, the analyses of the test results are carried out by three well known methods of slope stability analysis. One is the friction circle method (ϕ-circle method), and the other two are slice methods proposed by Fellenius and Bishop. Three solid curves already shown in Fig. 25 are the calculated failure envelopes in the V–H plane with $M=0$ and internal friction angle $\phi=45$ degree. The magnitude of the ϕ value is within the range of ϕ_{tr}, but is slightly higher than the average. The calculated failure envelopes by three different slip circle methods are amazingly different in shape. The solid circles in the figure are test data with negligible eccentricity as described previously. As is well known, the Fellenius method gives values too small, and the simplified Bishop method gives excessive bearing capacity on the V-load axis under vertical loading conditions, whereas the maximum horizontal load component calculated by these methods do not differ too much from each other. In the present case of a high mound with uniform material, the ϕ-circle method with the higher ϕ_{tr} ($\phi=45°$) gives the best fit.

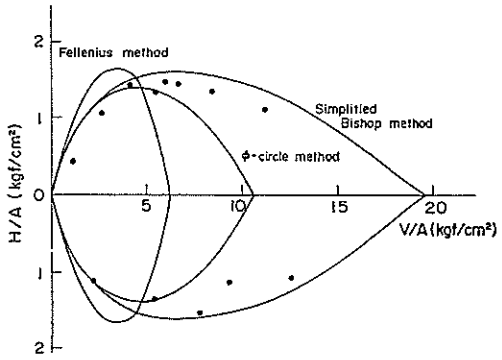

Fig. 28 Comparison of the test results with calculations by the average ϕ_{tr}

The ϕ value is corrected so as to fit the calculated failure loads with test data at the point which represents the maximum vertical bearing capacity. The fitted friction angles are 50 and 41 degrees for the Fellenius method and the simplified Bishop method respectively. The ϕ value obtained for the simplified Bishop method is smaller than average but within the range of ϕ_{tr}. The calculated bearing capacity by the simplified Bishop method is in good agreement with the test results. Whereas, although the fitted friction angle is used, the Fellenius method completely failed to explain the influence of the horizontal load component (load inclination). The horizontal load component of the calculated bearing capacity by the Fellenius method is more than twice that of the test results.

In the present model tests, Toyoura standard sand is used as the detailed characteristics including ϕ_{pl} are available. However, in the ordinary case encountered in practice, only the test data by the conventional triaxial compression tests are available at the best. Considering such an ordinary situation, a comparison is made between the model test results and the calculation using the average ϕ_{tr} value of 43 degrees. As shown in Fig. 28, the Fellenius method again failed to explain the test results. The simplified Bishop gives the best fit in this condition as long as the H/V is larger than 0.1.

In the comparison of the test results and the calculated bearing capacity, the internal friction angle ϕ has to be precisely determined. All the present model tests are carried out in the plane strain condition. It seems to be rigorous to use the ϕ value which is higher than the average ϕ_{tr} and which can represent the plane strain condition. From this view point, among the three simple slope stability analyses, the ϕ-circle method is considered to be the superior method to estimate the bearing capacity of the high mound.

As a routine design practice, however, it is most desirable to find out a combination of a simple analytical method and simple strength parameters obtainable by means of conventional soil tests such as ϕ_{tr}. The ϕ-circle method is not applicable to the two layered problem, where the mound height is not so high that the bearing capacity might be influenced by the flat ground under the mound. The simplified Bishop method with the average ϕ_{tr} is convenient for routine design practice and is able to cover a wide variety of geometric configurations of mound and sub-soil.

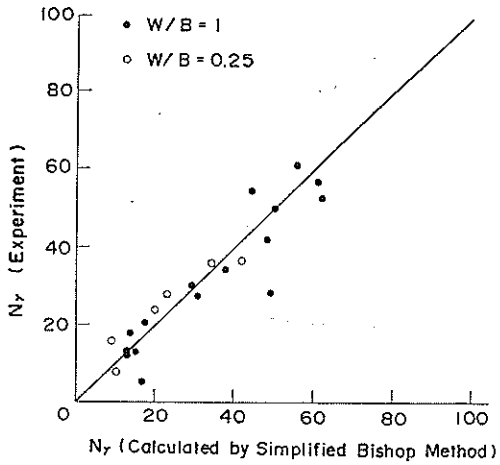

Fig. 29 Comparison of N_γ between the test results and the simplified Bishop method

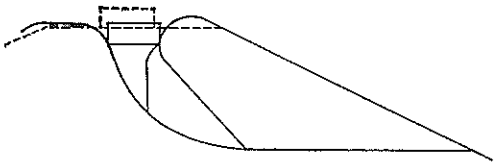

Fig. 30 Slip Surface for $e=0$ obtained by *X*-Photographs (at high vertical stress level)

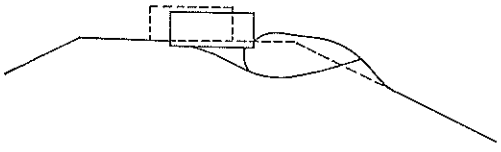

Fig. 31 Slip Surfaces for $e=0$ Obtained by *X*-ray Photographs (at low vertical stress level)

To investigate the applicability of the simplified Bishop method to the other geometric conditions, the comparison of the calculations with ϕ of 43 degree are made for all the test data. For the convenience of comparing different cases, the bearing capacity factor N_γ for the vertical load component at failure obtained by the model tests and the N_γ by the calculations are compared. As shown in Fig. 29, the Bishop method with the average ϕ_{tr} is confirmed to have the practically sufficient accuracy for different W/B and for wide range of eccentricity. The actual and calculated bearing capacity of the foundation is influenced by factors such as strength anisotropy, progressive failure, the difference of ϕ_{tr} and ϕ_{pl}, the error due to the over-simplification in the analytical technique, and etc. The reason why the simplified Bishop used with the average ϕ_{tr} gives a good coincidence with the actual behavior is probably due to the cancellation of these various factors which are not considered.

(2) Shape of Slip Surface in the Mound

For some cases, X-ray photographs are taken after the test. On these X-ray photographs, an image of a slip surface can be read due to the difference in the

density of sand caused by dilation. Figures 30 and 31 show the slip surfaces obtained for the higher and lower vertical load levels. For the higher vertical load level, the actual slip surface is far from a circular arc and can be approximated by the three parts as a wedge, logarithmic spiral and plane. For the lower vertical load level, the actual slip surface appears at the shallower depth in comparison with the slope circle obtained by the calculation. Even though the slip circle method using a triaxial ϕ value gives a good estimation of the failure load for practical purposes, the shape of the actual slip surface does not necessarily agree with that from the calculation. Further study is required to make a more rigorous explanation of the failure mechanism of the foundation on mounds in order to satisfy scientific interest, in the application of more sophisticated upper bound solution for the mound under the eccentric inclined loading, etc.

5. Field Loading Tests

5.1 Loading Test at Onahama Port

At Onahama port, a large scale field loading test was carried out using a prototype caisson. Figure 32 shows the plan and the cross section view of the test. To give an inclined and eccentric load to a rubble, a horizontal load was applied by hydraulic jacks placed on the existing breakwater. Four loading tests were performed where the widths of the rubble shoulders were changed from 5 to 25 m keeping the other conditions the same.

Figure 33 shows the relationship between the horizontal loads and rotational angles of the caisson for each test. As shown in this figure, horizontal loads increase gradually as the deformation of the caisson proceeds, and no clear peak value was observed.

Figure 34 shows the time relationship of the horizontal load and the horizontal deformation of the caisson. It can be seen that the horizontal deformation increases even under constant load. This appears to be due to the time dependency of rubble which was described in the discussion of the results of triaxial test for rubbles.

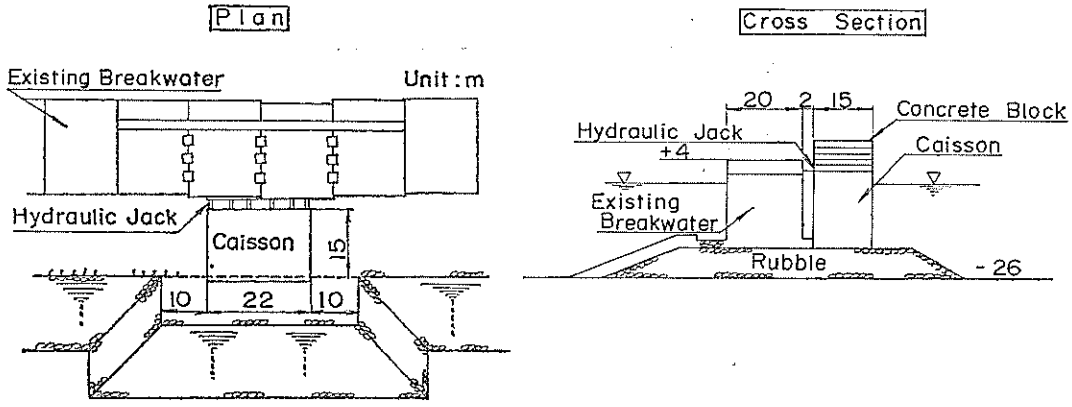

Fig. 32 Field Loading Test at Onahama Port

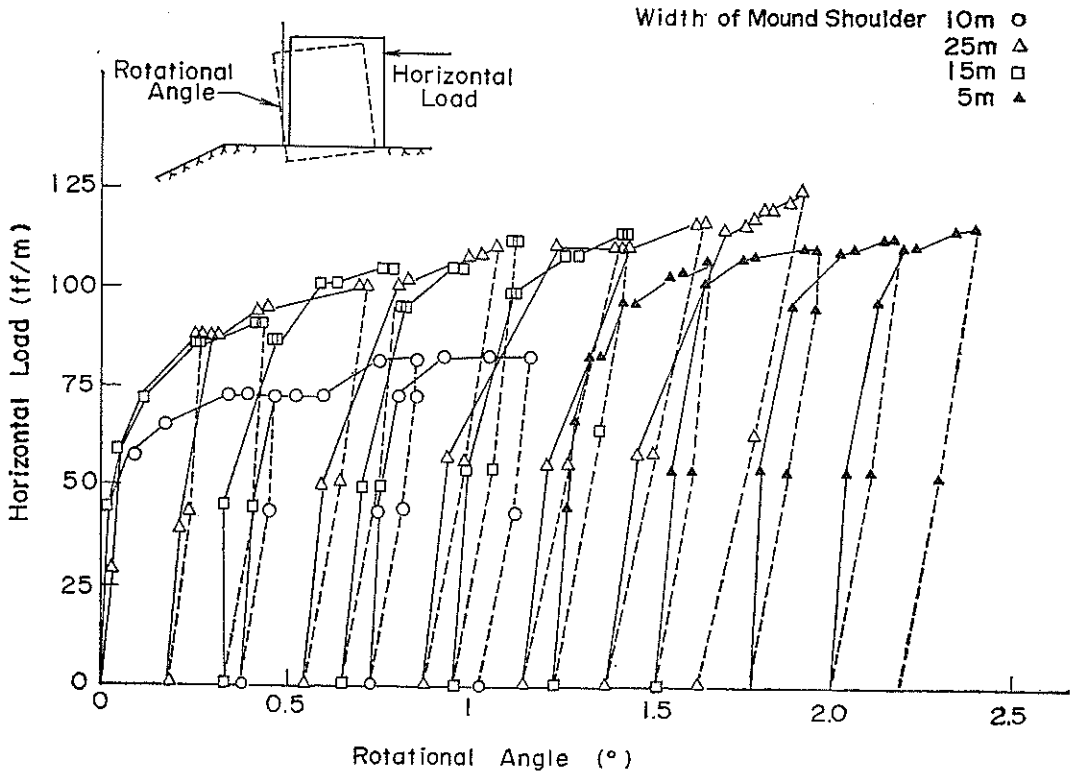

Fig. 33 Relationship between Horizontal Loads and Rotational Angle

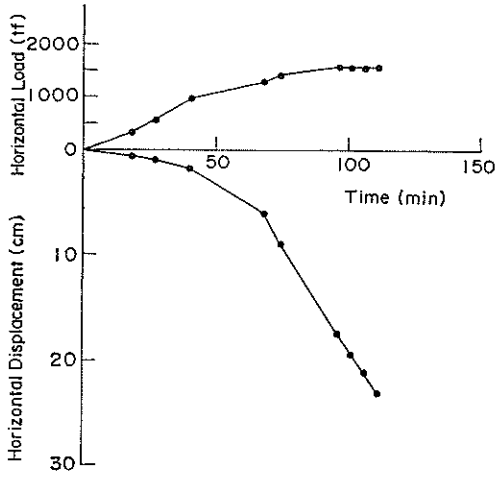

Fig. 34 Time Relationship of Horizontal Load and Horizontal Displacement

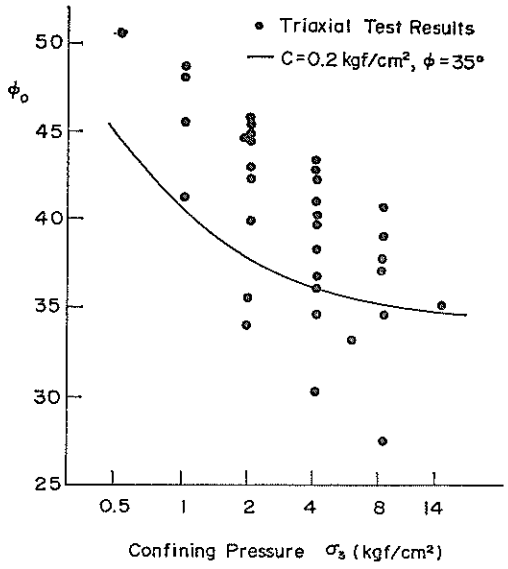

Fig. 35 Relationship between ϕ_0 and σ_3 (Apparent Cohesion is taken into account)

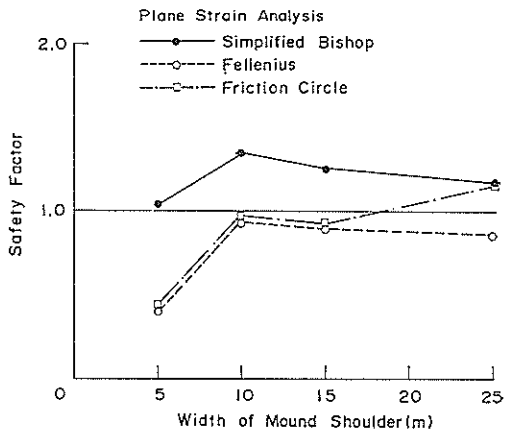

Fig. 36 Safety Factors by Various Methods (Two Dimensional Analysis)

Various stability analyses were carried out, i.e., the Fellenius method, the friction circle method and the simplified Bishop method. In the Fellenius method and the friction circle method, ϕ is raised 5°, on the basis of the vertification of damaged and undamaged prototype breakwaters. In the simplified Bishop method, the apparent cohesion $c=2\,\mathrm{tf/m^2}$ and $\phi=35°$ are employed similarly to the analysis of the large scale model test. As described above, the confining pressure dependency of rubble can be reproduced by introducing the apparent cohesion. In Fig. 35, the results of triaxial tests are compared with the proposed shear strength parameters $c=2\,\mathrm{tf/m^2}$ and $\phi=35°$. As shown in this figure, the proposed values seem to give an average, with yet slightly conservative strength.

At this location, the sub-soil is clean sand with shear strength parameters obtained by triaxial tests. In the simplified Bishop method, these parameters were used directly whereas empirical values based on the back analysis were used in the Fellenius method and the friction circle method.

Figure 36 shows the safety factors for each stability analysis. Here, the maximum horizontal loads of each loading test were used to calculate the safety factors. As shown in this figure, the simplified Bishop method gives safety factors that are too high, whereas the Fellenius method and the friction circle method give reasonable values close to unity.

However, it should be noted that this loading test was never carried out under the plane strain condition which is assumed in three stability analyses used here. As is well known, the ultimate bearing capacity of sand or rubble has a maximum value under the plane strain condition and decrease with the three dimensional effect. Thus, the results of the loading test tend to underestimate the bearing

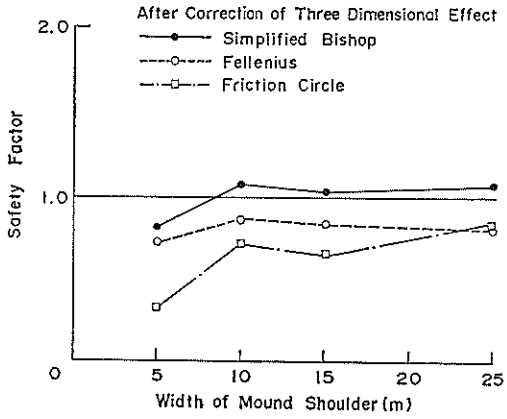

Fig. 37 Safety Factors by Various Methods (After Correction of Three Dimensional Effect)

capacity under the plane strain condition. The equation proposed by Vesić[15] was used to correct the three dimensional effect. In his equation, the bearing capacity is proportional to the value $(1.0–0.4\ B/L)$ where B and L are the breadth and the length of the foundation respectively. In the loading test, this value is 0.73. Therefore, the maximum horizontal loads should be raised to 1/0.73 times those of the loading test.

Figure 37 shows the results for the safety factors after correcting for the three dimensional effect. As shown in this figure, the simplified Bishop method give safety factors close to unity while other two methods give values that are too conservative. Thus the simplified Bishop method appears to give reasonable results if the apparent cohesion of rubble and the three dimensional effect are properly taken into account.

5.2 Loading Test at Yokohama Port

An onshore field loading test was carried out at Yokohama port. Figure 38 shows the outline of the test. A model mound was constructed on the foundation. By using hydraulic jacks, both vertical and horizontal loads were applied to the concrete block on the rubble mound. Although this loading test is small in scale when compared with that at Onahama port, it has the advantage that a number of tests were able to be carried out for various loading conditions. Two series of tests were performed: the first one was a bearing capacity test where a load inclination angle was small with a large eccentricity; the second one is a sliding test where a load inclination angle was large with a small eccentricity.

Figures 39 and 40 shows the safety factors of the bearing capacity test and the sliding test. They were obtained by three stability analyses using procedures similar to the analysis of the loading test at Onahama port. Thus, the apparent cohesion of rubble was introduced and the results of triaxial tests for sub-soil was directly utilized in the simplified Bishop method, whereas empirical values were used in other two methods. However, the effect of three dimensions is not taken into account for the Yokohama test results because the boundary conditions at Yokohama port

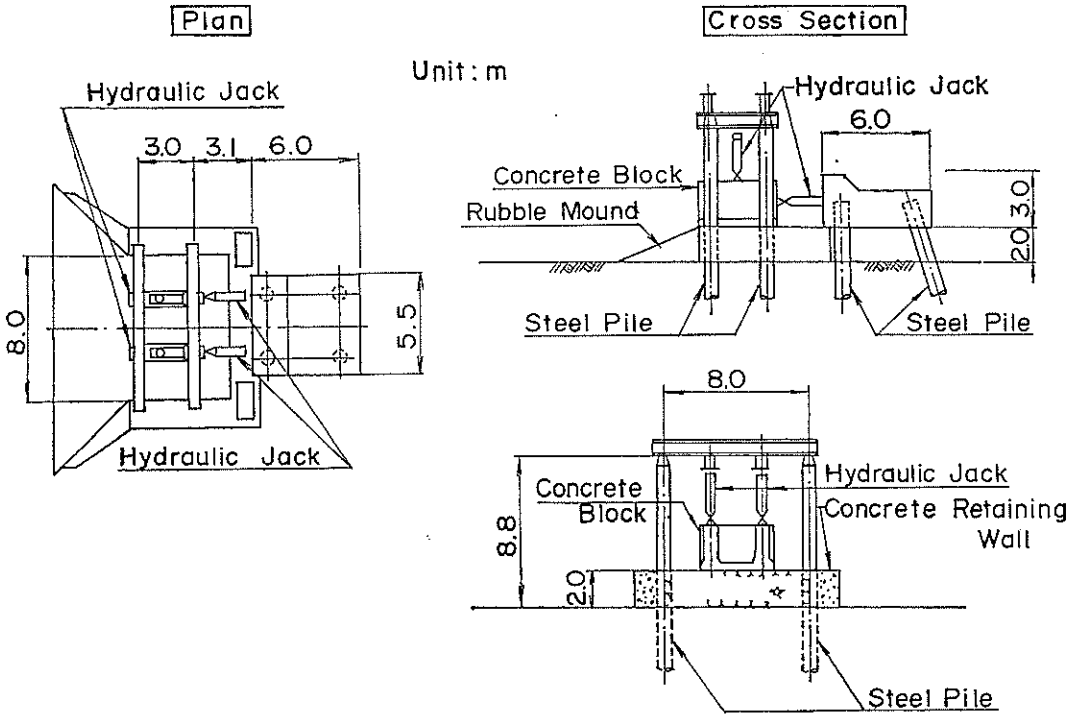

Fig. 38 Field Loading Test at Yokohama Port

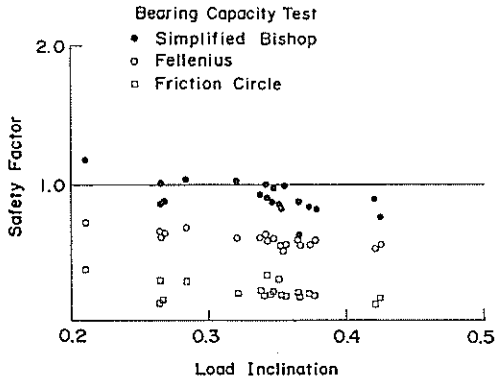

Fig. 39 Relationship between Safety Factors and Load Inclination (Bearing Capacity Test)

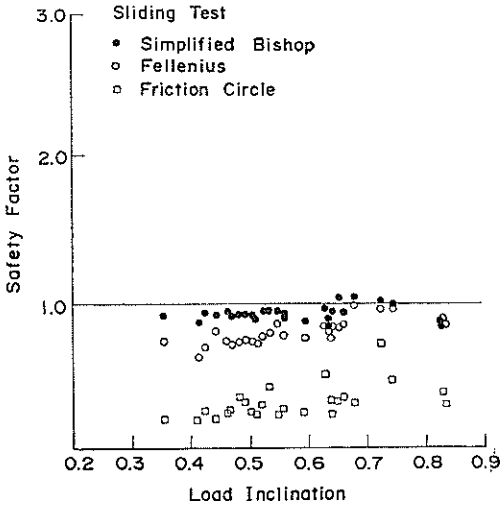

Fig. 40 Relationship between Safety Factors and Load Inclination (Sliding Test)

is not as clear as those at Onahama port. As shown in these figures, the simplified Bishop method gives the most reliable safety factors close to unity while other methods give values that are too small.

6. New Method for Calculating Bearing Capacity of Rubber Mound

6.1 Proposal of New Method

By carrying out various stability analyses for the large model test, the centrifuge test and the field loading test, it was shown that the simplified Bishop method gives the most reasonable results. Therefore we propose the simplified Bishop method as the standard procedure to calculate the bearing capacity of a gravity structure on a rubble mound. This new method can eliminate the highly empirical and yet complicated procedures which have been widely used in Japan.

The accuracy of the estimation for the bearing capacity depends not only on the method of the stability analysis but also on the determination of shear strength parameters. Based on the results of large triaxial tests, we propose the introduction of the apparent cohesion for rubbles. The apparent cohesion c and the angle of shear resistance ϕ varies with a number of factors such as the strength of rubble itself, the grain size distribution and the density in the field. However, at present there is no convenient method to obtain the shear strength parameters for rubble. Thus, we propose $c=2\,\mathrm{tf/m^2}$ and $\phi=35°$ as the standard value. These values can be used for normal rubble which is widely used in Japanese harbour construction.

As for the internal angle of friction ϕ of sand, the N value from the standard penetration test has been frequently used in Japan. We also propose a new method to predict ϕ where the effect of the overburden pressure is taken into account. Figure 41 shows the relationship between the N value and the relative density D_r for various overburden pressures. As shown in this figure, we have different D_r for the

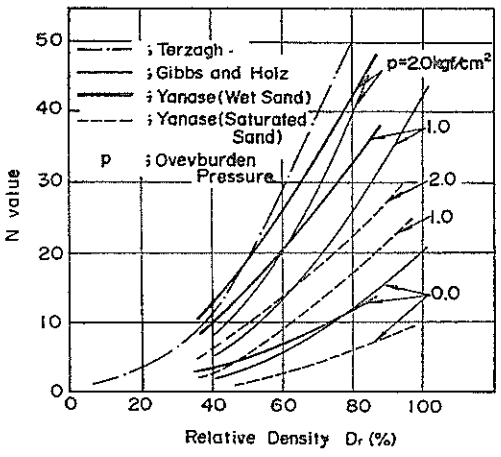

Fig. 41 Relationship between N value and Relative Density for Various Overburden Pressure

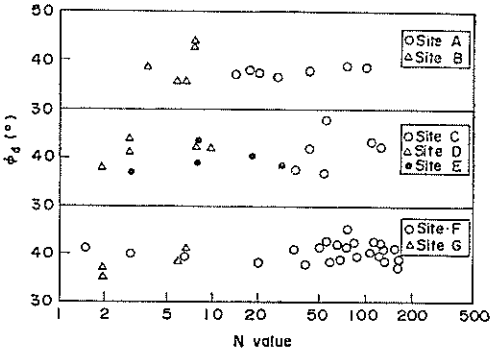

Fig. 42 Relationship between ϕ_d and N Value

same N value if the overburden pressure is different. Thus, we have to correct the effect of the overburden pressure to predict ϕ. However, because simpler procedure is preferred from the practical point of view, we propose a convenient method to get ϕ based on Fig. 42. This figure shows the relationship between ϕ obtained by triaxial tests and N values for various Japanese undisturbed sands. As shown in this figure, ϕ of sands does not largely depend on the N value due to the effect of the overburden pressure. Considering the difficulties of performing a triaxial test for undisturbed sand, we propose $\phi=40°$ for sand whose N value is below 10, and $\phi=45°$ for sand where the N value is above 10.

6.2 Verification of New Method with Prototype Data

Stability analyses based on the newly proposed method were carried out for actual structures. A number of gravity structures where the stability under inclined and eccentric loading was critical were compiled. Table 3 lists 19 breakwaters damaged by storms. While on the other hand, Table 4 shows a list of 10 breakwaters where no damage was recorded even though large wave forces must have been exerted. Of these breakwaters, there are 19 breakwaters where the safety factors for sliding were below unity. Bearing capacity analyses become meaningless for structures where the safety factors for sliding are below unity. Thus, verification of prototype breakwaters were carried out for the remaining 10 breakwaters whose safety factors for sliding were above unity.

Figure 43 shows the relationship between the safety factors derived from the Fellenius method and the caisson width of both damaged and undamaged break-

Table 3 List of Damaged Breakwaters

No.	Caisson width (m)	Mound depth (m)	Load Eccentricity	Load inclination	Toe pressure (tf/m^2)
1	10.0	2.0	0.450	1.095	55.3
2	13.0	2.0	0.237	0.661	13.6
2	11.0	1.2	0.352	0.613	49.8
4	15.0	1.4	※	1.453	※
5	15.0	2.5	0.229	0.705	10.0
6	10.5	2.2	0.472	1.003	121.0
7	16.0	2.5	0.174	0.441	24.2
8	15.0	6.0	0.321	0.710	47.7
9	15.0	8.0	0.271	0.593	32.5
10	18.0	4.5	0.407	0.837	74.1
11	17.0	5.5	0.321	0.621	58.2
12	20.0	5.0	0.299	0.584	49.6
13	20.0	7.0	0.283	0.573	48.6
14	8.0	3.6	※	2.479	※
15	5.0	1.5	※	2.564	※
16	14.0	2.5	0.147	0.349	18.3
17	22.0	3.5	0.353	0.723	91.4
18	13.0	5.7	0.503	0.871	※
19	17.0	4.0	0.375	0.691	90.2

Table 4 List of Undamaged Breakwaters

No.	Caisson width (m)	Mound depth (m)	Load Eccentricity	Load inclination	Toe pressure (tf/m^2)
1	15.0	5.0	0.417	0.726	140.4
2	18.0	2.0	0.317	0.555	68.3
3	18.5	3.0	0.213	0.505	61.9
4	17.0	6.5	0.298	0.632	47.6
5	9.0	10.0	0.266	0.436	28.1
6	13.0	2.0	0.355	0.676	53.4
7	10.6	5.0	0.388	0.554	80.1
8	7.0	2.0	0.491	0.620	862.6
9	9.6	1.0	0.225	0.444	23.7
10	12.0	2.5	0.306	0.545	48.2

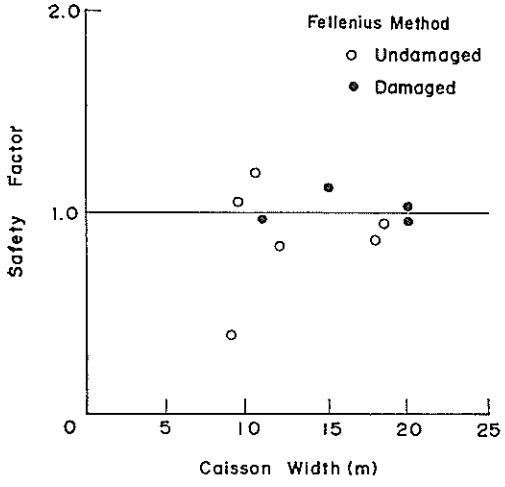

Fig. 43 Relationship between Safety Factors and Caisson Width of Breakwaters (Fellenius Method)

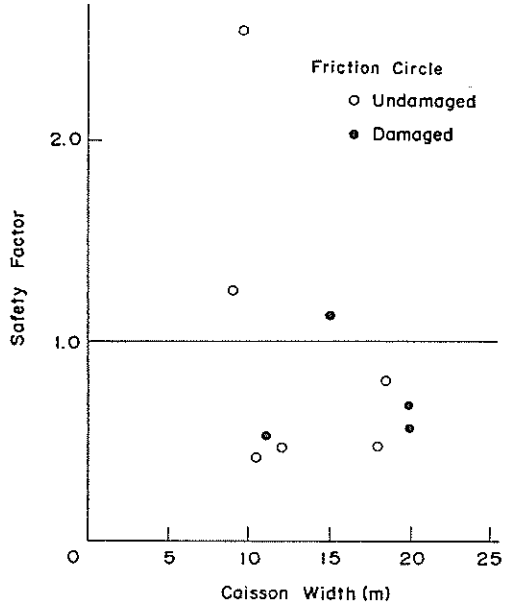

Fig. 44 Relationship between Safety Factors and Caisson Width of Breakwaters (Friction Circle Method)

waters. In this analysis, the shear strength parameters were modified on the basis of the past experience, similarly to the analysis of the field bearing tests. Figure 44 shows the similar results on the basis of the friction circle method. The same shear strength parameters as those for the Fellenius method were used. Figure 45 shows the results derived from the proposed method. In all these figures, damaged breakwaters are shown as closed circles and undamaged breakwaters are shown as open circles. By comparing Figs. 43–45, it can be seen that the newly proposed method gives

Table 5 List of Damaged and Undamaged Wharves

No.	Caisson width (m)	Mound depth (m)	Toe pressure (tf/m^2)	Damaged or Undamaged
1	6.1	1.0	60.0	Damaged
2	5.8	1.0	45.0	Damaged
3	6.3	1.7	27.0	Undamaged
4	3.2	1.0	38.0	Damaged
5	3.5	1.0	53.0	Damaged
6	4.5	0.7	23.0	Damaged
7	4.8	1.0	22.0	Damaged
8	2.8	1.0	12.0	Undamaged
9	5.0	1.0	33.0	Damaged
10	7.5	2.5	45.0	Damaged
11	5.7	1.5	41.0	Undamaged
12	9.0	1.5	47.0	Undamaged
13	6.5	5.0	48.0	Damaged
14	3.5	1.0	85.0	Damaged
15	4.5	1.0	52.0	Damaged
16	2.5	1.2	32.0	Damaged
17	3.0	1.0	31.0	Damaged

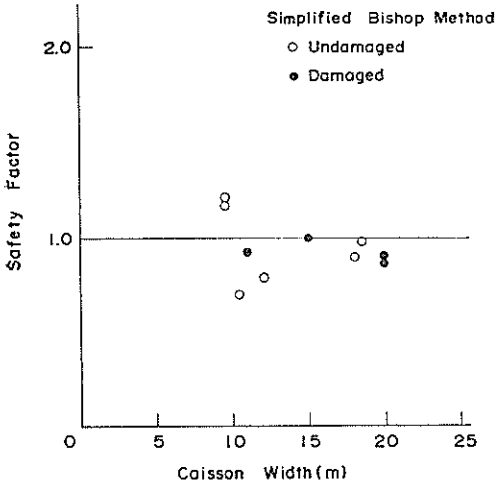

Fig. 45 Relationship between Safety Factors and Caisson Width of Breakwaters (Simplified Bishop Method)

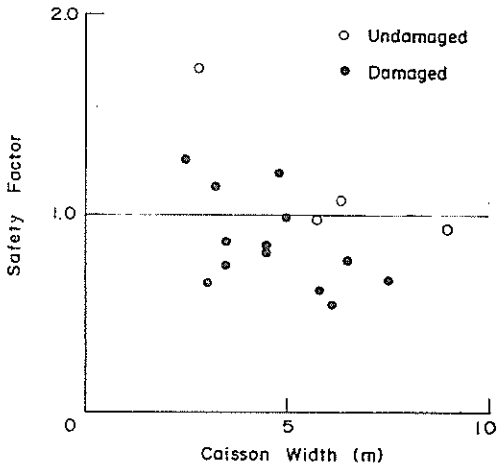

Fig. 46 Relationship between Safety Factors and Caisson Width of Wharves Simplified Bishop Method)

the most reasonable results because the proposed method gives safety factors below unity for all damaged breakwaters. Although there are a few undamaged breakwaters where the safety factors are below unity, they can be attributed to the slight conservative estimation of the shear strength of rubble without laboratory tests.

If the shear strength parameters of rubbles can be predicted more accurately by appropriate procedures, the simplified Bishop method will certainly give improved values.

Table 5 lists damaged and undamaged gravity wharves under earthquake conditions. Figure 46 shows the relationship between the safety factors of the proposed method and the wall width of wharves with closed circles for damaged wharves and open circles for undamaged wharves. Although there is a slight intermixing of damaged and undamaged data at the line of a safety factor=1.0, the proposed method also gives reasonable safety factors for wharves.

7. Conclusions

Extensive research was carried out to clarify the bearing capacity of a gravity structure resting on rubble mounds. The conclusions are as follows:

1. The shear strength of rubble is largely dependent on the confining pressure. This can be approximately simulated by introducing apparent cohesion.
2. The ultimate bearing capacity by the simplified Bishop method agrees favourably with the results of both laboratory tests and field tests.
3. Damaged and undamaged structures of composite breakwaters and gravity type wharves were examined. The simplified Bishop method gave reasonable results.
4. The simplified Bishop method can be used for the unified formula for calculating the bearing capacity of a rubble mound including sub-soil under eccentric and inclined loads. In this case, it is recommended to introduce the apparent cohesion for rubble.

(Received on November 13, 1987)

Acknowledgemens

This study was carried out in conjunction with the Second District Port Construction Bureau that performed field loading tests at Onahama port and Yokohama port. The authors wish to thank the many people who are responsible for the success of the difficult loading tests in the field.

References

1) Bureau of Ports and Harbours: Technical Standards for Port and Harbour Facilities in Japan, 1980.
2) KATAYAMA, T. and UCHIDA, T.: The Bearing Capacity of Strip Foundation on a Two-Layer Sandy Subsoil under Eccentric and Inclined Loads, *Technical Note of PHRI*, No. 140, 1972. (in Japanese)
3) UEZONO, A. and ODANI, H.: Design and construction of a rubble mound at great water depths—Kamaishi Breakwater, Tsuchi-to-Kiso, *JSSMFE*, Vol. 35, No. 3, 1987. (in Japanese)
4) SHOJI, Y.: Study of Shearing Properties of Rubbles with Large Scale Triaxial Compression Test, *Rept. of PHRI*, Vol. 22, No. 4, 1983. (in Japanese)
5) The Japanese Society of Soil Mechanics and Fountain Engineering: *Test and Design Strength of Rockfill Materials*,1982. (in Japanese)
6) LADD, C. C., FOOTT, R., ISHIHARA, K., SCHLOSSER, F. and POULOS, H. G.: Stress De-

formation and Strength Characteristics, State-of-the-Art Report, Session 1, *Proc. 9th ICSMFE*, Tokyo, Vol. 2, 1977.

7) ADACHR, T. and TATSUOKA, *F.*: *Soil Mechanics (3)—Consolidation, Shear, Dynamic Analysis—*, New Civil Engineering Series 18, Gihodo Publishing Co., 1981 (in Japanese).

8) MARSAL, R. J.: Mechanical Properties of Rockfill *Casagrande Volume*, John *Wiley* and Sons, 1972.

9) TAKAHASHI, K. and KASUGAI, Y.: Influence of Texture and Maximum Grain Size on Mechanical Properties of Rubbles, *Proceedings of the Symposium on Deformation and Strength Characteristics and Testing Method Coarse Granular Materials*, The Japanese Society of Soil Mechanics and Foundation Engineering, 1986. (in Japanese).

10) TAKAHASHI, K. and TOMITA, Y.: Experimental Study on the Bearing Capacity of Rubble Mound, *Rept. of PHRI*, Vol. 24 No. 1, 1985. (in Japanese)

11) TERASHI, M. and KITAZUME, M.: Bearing Capacity of a Foundation on Top of High Mound Subjected to Eccentric and Inclined Load, *Report of Port & Harbour Research Institute*, Vol. 26, No. 2, 1987.

12) TERASHI, M.: Development of PHRI Geotechnical Centrifuge and Its Application, *Report of Port & Harbour Research Institute*, Vol. 24, No. 3, 1985.

13) FUJI-I, N.: Studies on the Mechanism of Bearing Capacity of Shallow Footings by Centrifugal Model Tests, Doctoral Thesis, Tokyo Institute of Technology, 1976.

14) TERASHI, M., KITAZUME, M. and TANAKA, H.: Application of PHRI Geotechnical Centrifuge, *Proc. Int. Symp. on Geotechnical Centrifuge Model Testing*, Tokyo, 1984.

15) VESIĆ, A. S.: Bearing Capacity of Shallow Foundation, Found. Engineering ed. by Winterkorn & Fung, van Nostrand Reinhold, 1975.

List of Symbols

A	:	cross sectional area of the model foundation base
B	:	width of the model foundation
B_{shear}	:	grain breakage index after Marsal
c	:	cohesion
D_{max}	:	maximum grain size
D_r	:	relative density
D_r'	:	relative density according to e_{max} and e_4
D_{10}	:	effective grain size
e	:	load eccentricity
e_{max}	:	maximum void ratio
e_{min}	:	minimum void ratio
e_4	:	void ratio obtained after 4 minutes compaction; defined as e_{min} in the present study
e_{50}	:	void ratio at 50% of relative density based on e_4
F_s	:	safety factor
H	:	horizontal load
H	:	mound height
H-Load	:	horizontal component of the load
L	:	length of foundation
M	:	moment around the center line of the foundation base
N	:	acceleration applied in the model test (g)
N	:	blow count of standard penetration test
N_γ	:	bearing capacity factor for self weight

P : composite load
p_l : calculated toe pressure
U_c : uniformity coefficient of sand
V : vertical load
V-Load : vertical component of the load
W : distance of the foundation from the edge of the slope
α : angle of load inclination
α_i : initial value of α
α_f : α at the last point of the test
δ : composite displacement of the loading plate
δ_h : horizontal displacement increment
δ_v : vertical displacement increment
ε : $2e/B$
ε_v : volumetric strain in the triaxial test sample
ε_{cr} : eccentricity ε at the maximum value of p_l
ε_1 : axial strain in the triaxial test sample
σ_1 : effective axial stress
σ_3 : effective confining pressure
ϕ : angle of internal friction
ϕ_d : angle of internal friction under drained condition
ϕ_{pl} : ϕ obtained by the plane strain shear test
ϕ_{tr} : ϕ obtained by the conventional triaxial test
ϕ_0 : $\sin\phi_0=\{(\sigma_1-\sigma_3)/(\sigma_1+\sigma_3)\}_f$